In silico investigation of the short QT syndrome, using human ventricle models incorporating electromechanical coupling

Ismail Adeniran[1], Jules C. Hancox[2] and Henggui Zhang[1,3]*

[1] Computational Biology, Biological Physics Group, School of Physics and Astronomy, The University of Manchester, Manchester, UK
[2] School of Physiology and Pharmacology, and Cardiovascular Research Laboratories, School of Medical Sciences, University of Bristol, Bristol, UK
[3] School of Computer Science and Technology, Harbin Institute of Technology, Harbin, China

Introduction: Genetic forms of the Short QT Syndrome (SQTS) arise due to cardiac ion channel mutations leading to accelerated ventricular repolarization, arrhythmias and sudden cardiac death. Results from experimental and simulation studies suggest that changes to refractoriness and tissue vulnerability produce a substrate favorable to re-entry. Potential electromechanical consequences of the SQTS are less well-understood. The aim of this study was to utilize electromechanically coupled human ventricle models to explore electromechanical consequences of the SQTS.

Methods and Results: The Rice et al. mechanical model was coupled to the ten Tusscher et al. ventricular cell model. Previously validated K$^+$ channel formulations for SQT variants 1 and 3 were incorporated. Functional effects of the SQTS mutations on $\left[Ca^{2+}\right]_i$ transients, sarcomere length shortening and contractile force at the single cell level were evaluated with and without the consideration of stretch-activated channel current (I_{sac}). Without I_{sac}, at a stimulation frequency of 1Hz, the SQTS mutations produced dramatic reductions in the amplitude of $\left[Ca^{2+}\right]_i$ transients, sarcomere length shortening and contractile force. When I_{sac} was incorporated, there was a considerable attenuation of the effects of SQTS-associated action potential shortening on Ca^{2+} transients, sarcomere shortening and contractile force. Single cell models were then incorporated into 3D human ventricular tissue models. The timing of maximum deformation was delayed in the SQTS setting compared to control.

Conclusion: The incorporation of I_{sac} appears to be an important consideration in modeling functional effects of SQT 1 and 3 mutations on cardiac electro-mechanical coupling. Whilst there is little evidence of profoundly impaired cardiac contractile function in SQTS patients, our 3D simulations correlate qualitatively with reported evidence for dissociation between ventricular repolarization and the end of mechanical systole.

Keywords: short QT syndrome, stretch-activated channel, mechanical contraction, 3D model, human ventricles

INTRODUCTION

The short QT syndrome (SQTS) was first recognized as a distinct clinical entity in 2000 (Gussak et al., 2000). It is characterized by an abnormally short QT interval on the ECG with a QT$_C$ interval of ~320 ms or less, tall and peaked T-waves, and increased $T_{peak} - T_{end}$ width (Anttonen et al., 2009; Patel and Pavri, 2009; Couderc and Lopes, 2010; Cross et al., 2011; Gollob et al., 2011). Patients usually have structurally normal hearts and affected families tend to exhibit histories of syncope, abbreviated atrial and ventricular refractory periods, as well as increased susceptibility to atrial and ventricular arrhythmias and sudden death (Gaita et al., 2003; Schimpf et al., 2005; Giustetto et al., 2006; Hancox et al., 2011).

There are currently six identified forms of the genetic SQTS (SQT1–SQT6). SQT1-3 result from *gain-of-function* mutations to K$^+$ channel subunits. For SQT1, these mutations are to the *KCNH2* (*hERG*) gene encoding the α-subunit of the rapidly-activating delayed rectifier K$^+$ channel I_{Kr} (Brugada et al., 2004; Hong et al., 2005a; Sun et al., 2011). The SQT2 variant arises from mutations to the *KCNQ1* gene encoding the α-subunit of the slowly-activating delayed rectifier K$^+$ channel I_{Ks} (Bellocq et al., 2004; Hong et al., 2005b), whilst SQT3 involves mutations to the *KCNJ2* gene encoding the Kir 2.1 protein, which underlie the inwardly-rectifying K$^+$ current I_{K1} (Priori et al., 2005; Hattori et al., 2011; Deo et al., 2013). SQT4–SQT6 are due, respectively, to *loss-of-function* mutations to the *CACNA1C*, *CACNB2b* (Antzelevitch et al., 2007) and *CACNA2D1* (Templin et al., 2011) genes encoding the α1C, β2b, and α2δ-1- subunits of the L-type Ca^{2+} channel.

Pro-arrhythmic mechanisms in the SQTS have been investigated through the application of K$^+$ channel openers to left ventricular wedge preparations (e.g., Extramiana and Antzelevitch,

2004; Patel and Antzelevitch, 2008). Data from these experiments have been suggestive of a role for amplified transmural dispersion of repolarization and abbreviation of effective refractory period in the arrhythmogenic substrate in the SQTS (e.g., Extramiana and Antzelevitch, 2004; Patel and Antzelevitch, 2008). However, at present there are no phenotypically accurate animal models of the SQTS, making *in silico* approaches attractive for exploring the consequences of identified SQTS mutations. Computer models have reproduced QT interval shortening produced by K$^+$ channel mutations in the syndrome (Zhang and Hancox, 2004; Priori et al., 2005; Weiss et al., 2005; Zhang et al., 2008; Adeniran et al., 2011, 2012; Deo et al., 2013). Using a Markov-model of the N588K-hERG SQT1 mutation based on experimental data from recombinant wild-type and N588K-hERG channels, we have recently shown that this SQT1 mutation reduces substrate size and increases tissue vulnerability to premature stimuli in order to facilitate and maintain re-entrant excitation waves in 2D and 3D tissue. We have also shown that the SQT3 D172N Kir2.1 mutation increases tissue vulnerability, alters excitability, stabilizes and accelerates re-entry (Adeniran et al., 2012).

Although the SQTS is an electrical disorder, the heart is both an electrical and mechanical organ and it is feasible, at least in principle, that abbreviated repolarization in the syndrome might influence the mechanical function of the heart. In SQTS patients, there is some evidence of significant dissociation between ventricular repolarization and the end of mechanical systole (Schimpf et al., 2008). All modeling studies to-date that have investigated arrhythmogenesis in the SQTS have utilized ventricular cell and tissue electrical models that do not consider mechanical properties (Zhang and Hancox, 2004; Priori et al., 2005; Weiss et al., 2005; Zhang et al., 2008; Adeniran et al., 2011, 2012; Deo et al., 2013). Through mechano-electric feedback, the heart is able to regulate its electrical activity in response to changes in contractility or volume load (Lab, 1982, 1996; Franz, 1996). This regulation is believed to occur through the activation of stretch-activated channels (SACs) (Taggart, 1996; Bett and Sachs, 1997; Hu and Sachs, 1997; Youm et al., 2005). As potential electromechanical consequences of the SQTS are incompletely understood, the present study was conducted in order: (1) to investigate the potential functional consequences of the SQTS on ventricular contraction at the single cell, tissue and organ levels in the presence and absence of a stretch-activated current (I_{sac}) and (2) to evaluate the relationship between ventricular repolarization and mechanical systole in the setting of the SQTS. In order to address these aims, established models of the SQT1 and SQT3 K$^+$-channel-linked SQTS variants (Adeniran et al., 2011, 2012) were coupled to a validated mechanical model (Rice et al., 2008).

MATERIALS AND METHODS

SQT1 (I_{Kr}) AND SQT3 (I_{K1}) FORMULATIONS

For SQT1, we used a biophysically-detailed Markov chain model formulation which incorporates the experimentally observed kinetic properties of wild-type (WT) and N588K-mutated hERG/I_{Kr} channel current at 37°C (Adeniran et al., 2011). For SQT3, we employed a biophysically-detailed Hodgkin-Huxley model formulation (Adeniran et al., 2012), which also

incorporates the experimentally observed kinetic properties of the D172N-mutant Kir 2.1 channel at 37°C.

ELECTROMECHANICAL MODEL

For electrophysiology, we utilized the ten Tusscher and Panfilov (TP) human ventricular single cell model (Ten Tusscher and Panfilov, 2006), which recapitulates human ventricular cell electrical and membrane channel properties and the transmural heterogeneity of ventricular action potential (AP) across the ventricular wall (Ten Tusscher et al., 2004; Ten Tusscher and Panfilov, 2006). The TP model was modified and updated in 2006 to incorporate newly available experimental data (Xia et al., 2006); these modifications were also employed in the present study. This approach mirrors that used in our recent studies of electrical consequences of the SQT1 and SQT3 mutations (Adeniran et al., 2011, 2012).

We used the Rice et al. myocyte contraction model (Rice et al., 2008) to describe the mechanics of a cardiac myocyte. This model was chosen as it is based on the cross-bridge cycling model of cardiac muscle contraction and is able to replicate a wide range of experimental data including steady-state force-sarcomere length (F-SL), force-calcium and sarcomere length-calcium relations (Rice et al., 2008).

The intracellular calcium concentration $\left[Ca^{2+}\right]_i$ from the electrophysiology model (EP) was used as the coupling link to the myofilament mechanics model (MM). $\left[Ca^{2+}\right]_i$ produced as dynamic output from the EP model during the time course of the AP served as input to the MM model from which the amount bound to troponin is calculated. The formulation of the myoplasmic Ca^{2+} concentration in the EP model is:

$$\frac{dCa_i}{dt} = Ca_{\text{ibufc}}\left(\frac{V_{sr}}{V_c}\left(I_{\text{leak}} - I_{\text{up}}\right) + I_{\text{xfer}}\right)$$
$$- C_m \frac{I_{\text{bca}} + I_{\text{pca}} - 2I_{\text{NaCa}}}{2V_c F} \tag{1}$$

where Ca_{ibufc} is the total cytoplasmic buffer concentration, V_{sr} is the sarcoplasmic reticulum (SR) volume, V_c is the cytoplasmic volume, I_{leak} is the SR Ca^{2+} leak current, I_{up} is the SR Ca^{2+} pump current, I_{xfer} is the diffusive Ca^{2+} current current between dyadic Ca^{2+} subspace and bulk cytoplasm, C_m is the membrane cell capacitance per unit surface area, I_{bCa} is the background Ca^{2+} current, I_{pCa} is the plateau Ca^{2+} current, I_{NaCa} is the Na$^+$/Ca^{2+} exchanger and F is the Faraday constant.

The flux of the binding of Ca^{2+} to troponin was incorporated into Equation 1 as follows:

$$\frac{dCa_i}{dt} = Ca_{\text{ibufc}}\left(\frac{V_{sr}}{V_c}\left(I_{\text{leak}} - I_{\text{up}}\right) + I_{\text{xfer}}\right)$$
$$- C_m \frac{I_{\text{bCa}} + I_{\text{pCa}} - 2I_{\text{NaCa}}}{2V_c F} - \frac{dTropTot_{\text{Ca}}}{dt} \times \frac{1}{1000} \tag{2}$$

where $\frac{dTropTot_{\text{Ca}}}{dt}$ is the rate of Ca^{2+} binding to troponin. The combination of all state variables from the EP model with the MM model and the substitution of (Equation 2) for (Equation 1) yielded a human ventricular myocyte electromechanical cell model.

STRETCH-ACTIVATED CURRENT

In accord with previous studies (Kohl and Sachs, 2001; Panfilov et al., 2005; Youm et al., 2005; Kuijpers, 2008; Lunze et al., 2010), we incorporated a stretch-activated current (I_{sac}) into the electromechanics model using the following formulation:

$$I_{sac} = G_{sac} \times P_m \times (V_m - E_{sac}) \tag{3}$$

where G_{sac} and E_{sac} are the maximum channel conductance and reversal potential of the SAC, respectively. In the electromechanics model, E_{sac} was typically set to 1 mV and describes the experimentally observed depolarizing effect of the channel (Kohl et al., 1999; Trayanova et al., 2004). V_m is the membrane potential and P_m is the channel's open probability modeled as:

$$P_m = \frac{1.0}{1 + e^{-\left(\frac{\varepsilon - \varepsilon_{1/2}}{k_e}\right)}} \tag{4}$$

where ε and $\varepsilon_{1/2}$ are the strain (with an explicit dependence on the sarcomere length) and half-activation strain, respectively, $K_e = 0.02$ (Zabel et al., 1996; Youm et al., 2005; Lunze et al., 2010) is the activation slope.

The SAC is assumed to be permeable to Na^+, K^+ and Ca^{2+} (Kamkin et al., 2000; Youm et al., 2005; Kuijpers, 2008) with I_{sac} therefore defined as:

$$I_{sac} = I_{sac,\ Na} + I_{sac,\ K} + I_{sac,\ Ca} \tag{5}$$

where $I_{sac,\ Na}$, $I_{sac,\ K}$, and $I_{sac,\ Ca}$ are the contributions of Na^+, K^+ and Ca^{2+} to I_{sac}. To evaluate the effects of the permeability of the SAC to Na^+, K^+, and Ca^{2+}, two permeability ratio cases were considered in the single cell simulations: $P_{Na} : P_K : P_{Ca} = 1:1:0$ and $P_{Na} : P_K : P_{Ca} = 1:1:1$ where P_{Na}, P_K, and P_{Ca} are the relative permeabilities of the channel to Na^+, K^+ and Ca^{2+}, respectively.

TISSUE MECHANICS MODEL

We modeled cardiac tissue mechanics within the theoretical framework of non-linear elasticity (Marsden and Hughes, 1994; Holzapfel, 2000) as an inhomogeneous, anisotropic, nearly incompressible non-linear material similar to previous studies (Hunter et al., 1997; Costa et al., 2001; Whiteley et al., 2007; Niederer and Smith, 2008; Pathmanathan and Whiteley, 2009). We used a two-field variational principle with the deformation u and the hydrostatic pressure p as the two fields (Lions and Ciarlet, 1994; Holzapfel, 2000; Bonet and Wood, 2008). p is utilized as the Lagrange multiplier to enforce the near incompressibility constraint. Thus, the total potential energy functional Π for the mechanics problem is formulated as:

$$\Pi(u, p) = \Pi_{int}(u, p) + \Pi_{ext}(u) \tag{6}$$

where $\Pi_{int}(u, p)$ is the internal potential energy or total strain energy of the body and $\Pi_{ext}(u)$ is the external potential energy or potential energy of the external loading of the body. With the axes of the geometry aligned to the underlying tissue microstructure (Seemann et al., 2006; Legrice et al., 1997), the second Piola-Kirchhoff stress tensor S, obtained from the directional derivative of Equation 6 in the direction of an arbitrary virtual displacement and which relates a stress to a strain measure (Holzapfel, 2000; Bonet and Wood, 2008) is defined as:

$$S = \frac{1}{2}\left(\frac{\partial W}{\partial E_{MN}} + \frac{\partial W}{\partial E_{NM}}\right) - pC_{MN}^{-1} + S_{ActiveTension} \tag{7}$$

where W is a strain energy function that defines the constitutive behavior of the material, E is the Green-Lagrange strain tensor that quantifies the length changes in a material fiber and angles between fiber pairs in a deformed solid, C is the Right-Cauchy green strain tensor, p is a Lagrange multiplier (referred to as the hydrostatic pressure in the literature) used to enforce incompressibility of the cardiac tissue, $S_{ActiveTension}$ is a stress tensor incorporating active tension from the electromechanics cell model and enables the reproduction of the three physiological movements of the ventricular wall: longitudinal shortening, wall thickening and rotational twisting (MacGowan et al., 1997; Lorenz et al., 2000; Tseng et al., 2000; Bogaert and Rademakers, 2001; Cheng et al., 2008; Coppola and Omens, 2008; Lilli et al., 2013).

For the strain energy function W, we used the Guccione constitutive law (Guccione et al., 1991) given by:

$$W = C_1 e^Q \tag{8}$$

Where

$$Q = C_2 E_{11}^2 + C_3\left(E_{22}^2 + E_{33}^2 + 2E_{23}^2\right) + 2C_4(E_{12}E_{21} + E_{13}E_{31}) \tag{9}$$

following previous work (Land et al., 2012), $C_1 = 0.831$ kPa, $C_2 = 14.31$, $C_3 = 4.49$, $C_4 = 10$. E_{ij} are the components of the Green-Lagrange strain tensor.

TISSUE ELECTROPHYSIOLOGY MODEL

The monodomain representation (Colli Franzone et al., 2005; Potse et al., 2006; Keener and Sneyd, 2008) of cardiac tissue was used for the electrophysiology model with a modification (the incorporation of the Right Cauchy Green deformation tensor C), which allows the monodomain equation to take into account the effect of the deforming tissue, similar to previous studies (Nash and Panfilov, 2004; Whiteley et al., 2007; Pathmanathan and Whiteley, 2009):

$$C_m \frac{dV}{dt} = -(I_{ion} + I_{stim}) + \nabla \times (DC^{-1}\nabla V) \tag{10}$$

where C_m is the cell capacitance per unit surface area, V is the membrane potential, I_{ion} is the sum of all transmembrane ionic currents from the electromechanics single cell model, I_{stim} is an externally applied stimulus and D is the diffusion tensor. In simulations, intracellular conductivities in the fiber, cross-fiber and sheet directions were set to 3.0, 1.0, and 0.31525 ms mm^{-1}, respectively. These gave a conduction velocity of 65 cm s^{-1} in the

fiber direction along multiple cells, which is close to the value 70 cm s^{-1} observed in the fiber direction in human myocardium (Taggart et al., 2000).

COMPUTATIONAL METHODS
Geometry and meshes
The 3D simulations were carried out on a DT-MRI reconstructed anatomical human ventricle geometry, incorporating anisotropic fiber orientation, from a healthy 34-year-old male. This had a spatial resolution of 0.2 mm and approximately 24.2 million nodes in total and was segmented into distinct ENDO (25%), MCELL (35%), and EPI (40%) regions. The chosen cell proportion in each region is similar to those used in other studies (Gima and Rudy, 2002; Zhang et al., 2008; Adeniran et al., 2011, 2012). The conditional activation sites were determined empirically across the ventricle wall and were validated by reproducing the activation sequence and QRS complex in the measured 64-channel ECG (Keller et al., 2009) of that person.

Solving the electromechanics problem
The electromechanics problem consists of two sub-problems: the electrophysiology problem and the mechanics problem. The electrophysiology problem (Equation 10) was solved with a Strang splitting method (Sundnes et al., 2005) ensuring that the solution is second-order accurate. It was discretized in time using the Crank-Nicholson method (Burnett, 1987), which is also second-order accurate and discretized in space with Finite Elements (Burnett, 1987; Braess, 2007; Brenner and Scott, 2010; Ern and Guermond, 2010). I_{ion} in (Equation 10) represents the single cell electromechanics model from which the active tension input to the Tissue mechanics model for contraction is obtained. The system of ordinary differential equations (ODE) composing I_{ion} was solved with a combination of the Rush-Larsen scheme (Rush and Larsen, 1978) and the CVODE solver (Cohen et al., 1996; Hindmarsh et al., 2005).

The mechanics problem (Equation 6) was also solved using the Finite element Method using the automated scientific computing library, FEniCS (Logg et al., 2012). The resulting non-linear system of equations was solved iteratively using the Newton method to determine the equilibrium configuration of the system. The value of the Right Cauchy Green Tensor C was then used to update the diffusion coefficient tensor in Equation 10. Over a typical finite element domain, P_2 elements (Braess, 2007; Brenner and Scott, 2010; Ern and Guermond, 2010) were used to discretize the displacement variable u, while the pressure variable p was discretized with P_1 elements (Braess, 2007; Brenner and Scott, 2010; Ern and Guermond, 2010). This $P_2–P_1$ mixed finite element has been proven to ensure stability (Chamberland et al., 2010; Haga et al., 2012; Logg et al., 2012) and an optimal convergence rate (Hughes, 2000; Chamberland et al., 2010; Ern and Guermond, 2010).

The algorithm for solving the full electromechanics problem is as follows:

1. Determine the initial deformation and obtain the value of the Right Cauchy Green Tensor C.
2. While time $< t_{end}$:

a. Solve the electrophysiology problem for $\Delta t_{mechanics} = 1$ ms with C as input and active tension T_a as output ($\Delta t_{electrophysiology} = 0.01$ ms).
b. Project T_a from the electrophysiology mesh onto the mechanics mesh.
c. Solve the mechanics problem with T_a as input and C as output.

RESULTS
SINGLE CELL ELECTROMECHANICAL SIMULATIONS
Simulations without incorporation of I_{sac}
Initial simulations, in the absence of I_{sac}, were performed using the coupled electromechanics model for the WT condition for each of ENDO, MCELL, and EPI conditions. **Figure 1** shows the electrophysiological consequences of the SQT1 and SQT3 mutations in EPI, MCELL, and ENDO cell types at a stimulation frequency of 1 Hz (**Figures 1Ai–Ci**). For the EPI cell, action potential duration at 90% repolarization (APD$_{90}$) was 317 ms under WT conditions and was shortened to 212 ms and 283 ms respectively under SQT1 and SQT3 conditions. For the MCELL, WT APD$_{90}$ was 441 ms, whilst it was 232 and 382 ms under SQT1 and SQT3 conditions, respectively. For the ENDO cell model, WT APD$_{90}$ was 317 ms, whilst it was 211 and 284 ms under SQT1 and SQT3 respectively. The observed APD shortening was more extensive for SQT1 than SQT3 and this is explicable on the basis of the relative timings and roles of I_{Kr} and I_{K1} during ventricular AP repolarization. As shown in **Figures 1Aii–Cii**, the SQT1 N588K mutation produced a large increase in I_{Kr} together with a change in the current's profile that resulted in a significant augmentation of I_{Kr} and shift in timing of maximal current to be earlier during the AP plateau (see also Adeniran et al., 2011). The D172N mutation significantly increased I_{K1} magnitude (**Figures 1 Aiii–Ciii**), but as I_{K1} contributes to terminal AP repolarization, the consequence of the mutation for APD shortening was less extensive than that for the SQT1 mutation. The electrophysiological consequences of the SQT1 and SQT3 mutations in these simulations are comparable to those reported previously from non-mechanically coupled ventricular cell models (Adeniran et al., 2011, 2012).

To validate the electromechanics model, we simulated force-frequency relationship (FFR) by stimulating the single cell at different frequencies for 1000 beats until steady state, recorded the maximum force developed and plotted it against frequency and compared it to experimental data (Mulieri et al., 1992). The results are shown in **Figure 2**. In the frequency range, 1–2 Hz, the electromechanics model produced an FFR which is qualitatively comparable to experimental data (vertical dashed lines) (Mulieri et al., 1992) and showed the Bowditch staircase or Treppe effect (Woodworth, 1902; Mulieri et al., 1992; Lakatta, 2004). All subsequent simulations in this study were carried out at 1 Hz. We then proceeded to characterize the calcium and contractile properties of the electromechanically coupled WT cell models. **Figure 3** shows the action potential (AP), $[Ca^{2+}]_i$ transient, sarcomere length shortening (SLs): EPI (**Figures 3Ai–Aiv**), MCELL (**Figures 3Bi–Biv**), and ENDO (**Figures 3Ci–Civ**). The larger $[Ca^{2+}]_i$ transient (and hence contraction) of the MCELL compared to EPI and ENDO cells is consistent with experimental data (McIntosh et al., 2000).
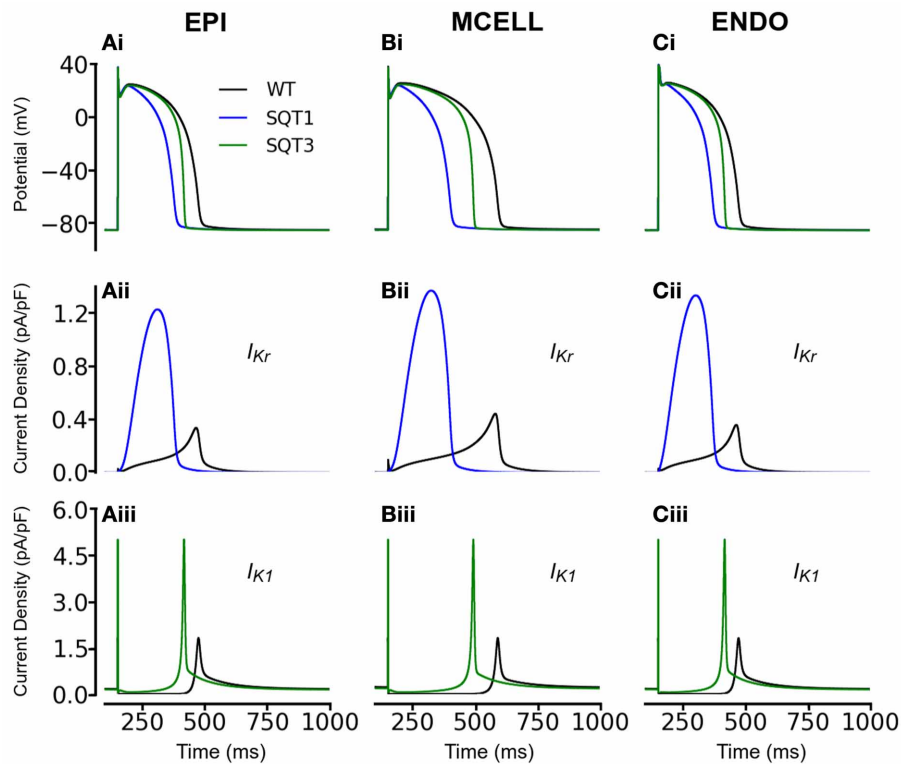
FIGURE 1 | Simulation of ventricular action potentials and the time course of I_{Kr} and I_{K1}. (Ai–Ci) Steady state (at a stimulation frequency of 1 Hz) action potentials for EPI **(Ai)**, MCELL **(Bi)**, and ENDO **(Ci)** cells under wild-type (WT; black), SQT1 (blue) and SQT3 (green) conditions. **(Aii–Cii)** Corresponding I_{Kr} current profiles for EPI **(Aii)**, MCELL **(Bii)**, and ENDO **(Cii)** cells under the WT (black) and SQT1 (blue) conditions. **(Aiii–Ciii)** Corresponding I_{K1} current profiles for EPI **(Aiii)**, MCELL **(Biii)**, and ENDO **(Ciii)** cells under the WT (black) and SQT1 (blue) conditions.
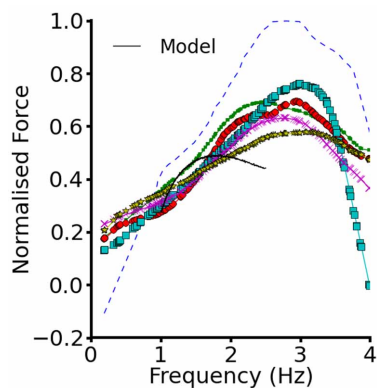

FIGURE 2 | Force-frequency relationship. Plot of steady state normalized active force vs. heart rate using the EPI cell model. Black continuous line represents the WT electromechanics model while symbols represent experimental data from non-failing control preprarations of human myocardium. Experimental data from Mulieri et al. (1992).

Figure 3 also shows the effects of incorporating the SQT1 and SQT3 mutations on the AP, $[Ca^{2+}]_i$ transient, SL shortening and active force in the coupled electromechanics single cell models. Both mutations shortened the AP (**Figures 3Ai–Ci**), reduced

the amplitude of $[Ca^{2+}]_i$ (**Figures 3Aii–Cii**) and SL shortening (**Figures 3Aiii–Ciii**) in each of the EPI, MCELL, and ENDO cell models. These effects led to the attenuation of contractility (percentage of WT) in all the cell types (**Figures 3Aiv–Civ**) (SQT1 EPI 30%; SQT3 EPI 76%; SQT1 MCELL 44%; SQT3 MCELL 83%; SQT1 ENDO 41%; SQT3 ENDO 78%). As identified in **Figure 1**, the effects for the SQT3 mutation were not as pronounced as the SQT1 mutation because of the relative timing of I_{Kr} and I_{K1} during the AP, with the SQT3 mutation influencing only terminal repolarization and consequently giving rise to longer APDs across the ventricular wall.

The observed reduction in the active force under the mutation conditions in **Figure 3** was profound, particularly in the case of SQT1. In order to elucidate the mechanism causing such a decrease in contractile force, we performed a simulated "AP clamp" experiment on the WT electromechanics model (**Figure 4**), using two different AP profiles—one AP of a normal duration and the other AP with an abbreviated duration. In this experiment, WT I_{Kr} and I_{K1} formulations were used, therefore any observed alterations to $[Ca^{2+}]_i$ and contractile force would relate to APD *per se*. **Figure 4A** shows the two AP clamp commands used. **Figure 4B** shows the AP-evoked I_{CaL} whilst **Figures 4C–E** respectively show $[Ca^{2+}]_i$, active force, and the difference in steady state level of free calcium concentration in the sarcoplasmic reticulum (CaSR). The results of these simulations

**FIGURE 3 | Single cell effects of the SQT1 and SQT3 mutations (without
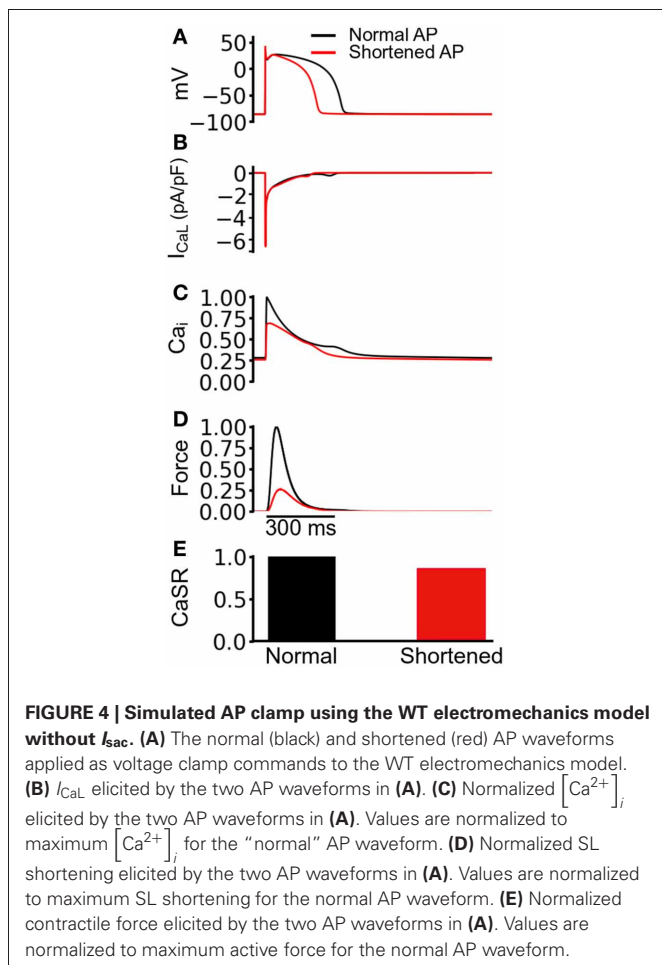I_{sac}). (Ai–Ci)** WT (black), SQT1 (blue) and SQT3 (green) action potentials in
the EPI **(Ai)**, MCELL **(Bi)**, and ENDO **(Ci)** cell models. **(Aii–Cii)** WT (black),
SQT1 (blue) and SQT3 (green) intracellular calcium concentration and Ca^{2+}
transients in the EPI **(Aii)**, MCELL **(Bii)**, and ENDO **(Cii)** cell models.

(Aiii–Ciii) WT (black), SQT1 (blue) and SQT3 (green) sarcomere length (SL) in
the EPI **(Aiii)**, MCELL **(Biii)**, and ENDO **(Ciii)** cell models. **(Aiv–Civ)** WT
(black), SQT1 (blue) and SQT3 (green) active force in the EPI **(Aiv)**, MCELL
(Biv), and ENDO **(Civ)** cell models. Values are normalized to WT maximum
active force for each cell type.

showed that though the shorter AP did not alter notably the
peak amplitude of I_{CaL}, it reduced the amplitude of the $[Ca^{2+}]_i$
transient, SL shortening and the active force and—notably—SR
calcium content (CaSR). These effects are similar to the results
shown in **Figure 3** for the SQT models. However, in the AP clamp
simulation, any observed reduction in amplitude of $[Ca^{2+}]_i$, SL
shortening, CaSR and the active force can be attributed solely to
consequences of application of the shorter AP waveform. This
suggests that the key reason for the reduced active force in the
SQTS setting (**Figure 3**) is the indirect effect of the SQT mutation-
linked AP shortening on Ca^{2+} handling (and on SR content in
particular).

To investigate further the functional impact of AP duration on
the loading of SR calcium content at the steady state, we applied
conditioning trains containing one of two different AP clamp
commands (one with a longer and the other with a shorter AP
duration) to the WT electromechanics model; the conditioning
train was followed by an identical single square voltage command
to +10 mV for 300 ms (**Figure 5A**). With the conditioning train
of APs comprised of the longer duration AP, it was observed that
the +10 mV square pulse command produced a larger $[Ca^{2+}]_i$

transient than that when conditioning trains of shorter duration
APs were applied. Results are shown in **Figure 5C**. With the con-
ditioning AP trains of different durations, the square pulse elicited
an identical I_{CaL} (**Figure 5B**), but a smaller $[Ca^{2+}]_i$ amplitude
(**Figure 5C**) and active force (**Figure 5D**) for the shorter dura-
tion AP. These simulations also showed that prior to the square
pulse command, the SR was filled to a greater level with the
longer duration conditioning APs than with those of shorter
duration,(as illustrated by the steady state CaSR in **Figure 5E**).
This further validates the notion that the attenuation of $[Ca^{2+}]_i$
amplitude and contractility with the SQT mutations was conse-
quent upon reduced SR content associated with abbreviation of
AP duration.

Incorporation of I_{sac}

We then performed comparable simulations with the incorpora-
tion of I_{sac}. **Figures 6, 7** show the results with the SAC assumed to
be permeable to Na^+, K^+ and Ca^{2+} in the ratio 1:1:0 (**Figure 6**)
and 1:1:1 (**Figure 7**). The resting potential for EPI, MCELL and
ENDO decreased from −86 to −76 mV (I_{sac} at 1:1:0 permeability
ratio) and to −79 mV (I_{sac} at 1:1:1 permeability ratio) for the WT

FIGURE 4 | Simulated AP clamp using the WT electromechanics model without I_{sac}. (A) The normal (black) and shortened (red) AP waveforms applied as voltage clamp commands to the WT electromechanics model. **(B)** I_{CaL} elicited by the two AP waveforms in **(A)**. **(C)** Normalized $\left[Ca^{2+}\right]_i$ elicited by the two AP waveforms in **(A)**. Values are normalized to maximum $\left[Ca^{2+}\right]_i$ for the "normal" AP waveform. **(D)** Normalized SL shortening elicited by the two AP waveforms in **(A)**. Values are normalized to maximum SL shortening for the normal AP waveform. **(E)** Normalized contractile force elicited by the two AP waveforms in **(A)**. Values are normalized to maximum active force for the normal AP waveform.

FIGURE 5 | Changes in steady state SR content induced by conditioning trains of action potentials of differing duration. (A) Protocol used to determine steady state SR content, comprised of train of 100 normal (black) and shortened (red) AP clamp commands followed by a 300 ms square command voltage pulse to +10 mV. **(B)** I_{CaL} elicited by the +10 mV voltage command. Peak I_{CaL} is equal with the two AP waveforms in **(A)**. **(C)** Normalized $\left[Ca^{2+}\right]_i$ elicited by the by the +10 mV voltage command. Values are normalized to maximum $\left[Ca^{2+}\right]_i$ for the "normal" AP waveform. **(D)** Normalized active force elicited by the +10 mV voltage command. Values are normalized to maximum active force for the normal AP waveform. **(E)** Normalized maximum SR Ca^{2+} content prior to the application of +10 mV voltage command in **(A)**. Values are normalized to maximum SR Ca^{2+} for the normal AP waveform.
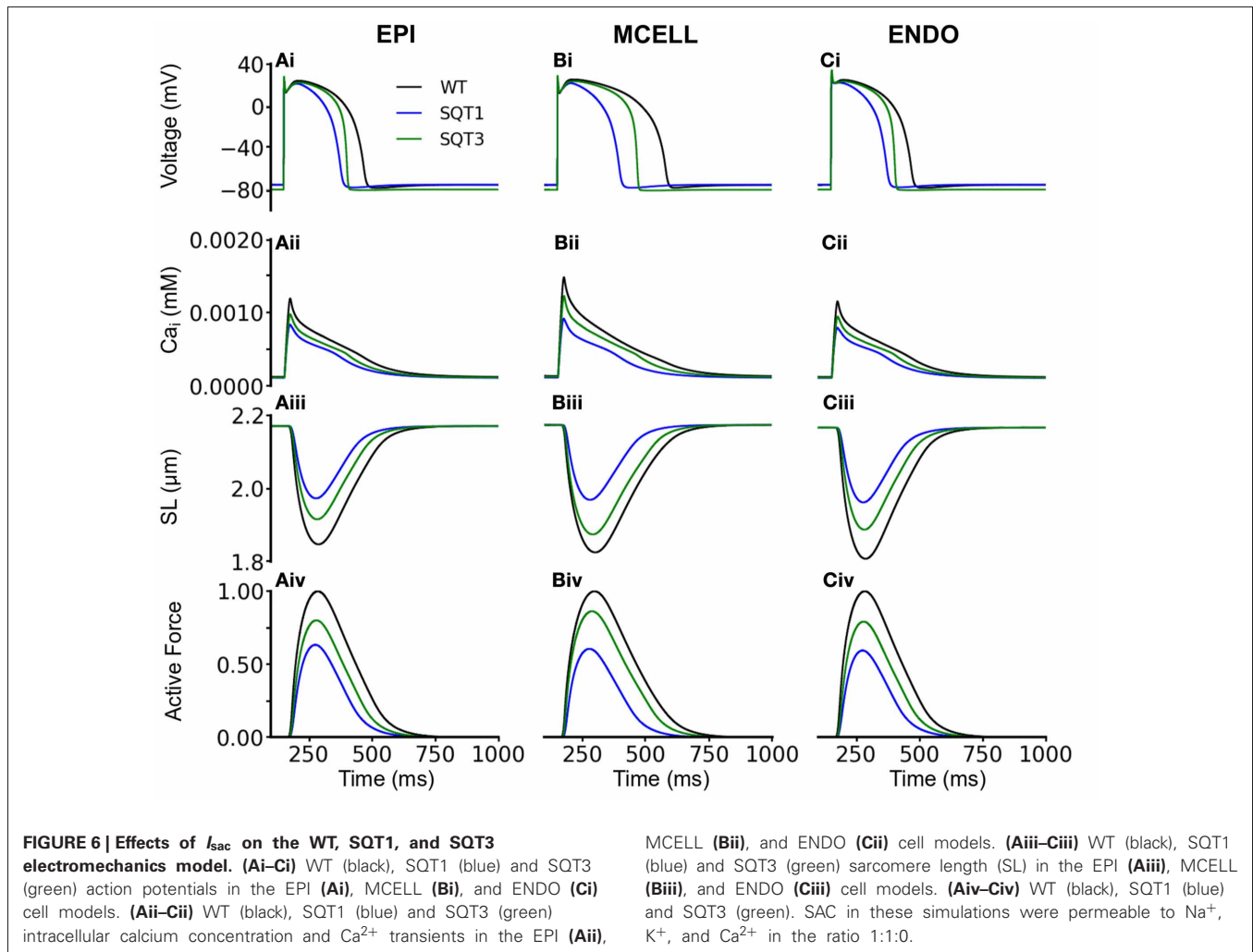
and SQT1 conditions respectively. Depolarization of the membrane potential is an effect of SACs, which has been observed experimentally (Boland and Troquet, 1980; Franz et al., 1992; Kamkin et al., 2000). The resting membrane potential remained unchanged under the SQT3 condition because the increase in outward I_{K1} caused by the mutation counteracted the depolarizing effect of I_{sac}. Similar to the situation without I_{sac}, the incorporation of SQT1 and SQT3 mutations abbreviated the AP in all three cell types (**Figures 6Ai–Ci, 7Ai–Ci**). The most significant consequences of inclusion of I_{sac} were upon $\left[Ca^{2+}\right]_i$ and contractile activity. Thus, the results shown in **Figures 6, 7** indicate that incorporation of I_{sac} attenuated the reduction caused by the SQT1 and SQT3 mutations shown in **Figure 3** on $\left[Ca^{2+}\right]_i$ (**Figures 6Aii–Cii, 7Aii–Cii**), SLs (**Figures 6Aiii–Ciii, 7Aiii–Ciii**) and active force (**Figures 6Aiv–Civ, 7Aiv–Civ**). I_{sac} incorporated at 1:1:1 permeability ratio (i.e., incorporating Ca^{2+} permeability) produced the greater effect, with contractility across the ventricular wall being approximately 85% of control under the SQT1 mutation and 92% of control under the SQT3 mutation. In contrast, with I_{sac} incorporated at a permeability ratio of 1:1:0, on average across the ventricular wall, the contractile force was 62% of control under the SQT1 condition and 82% of control under the SQT3 condition.
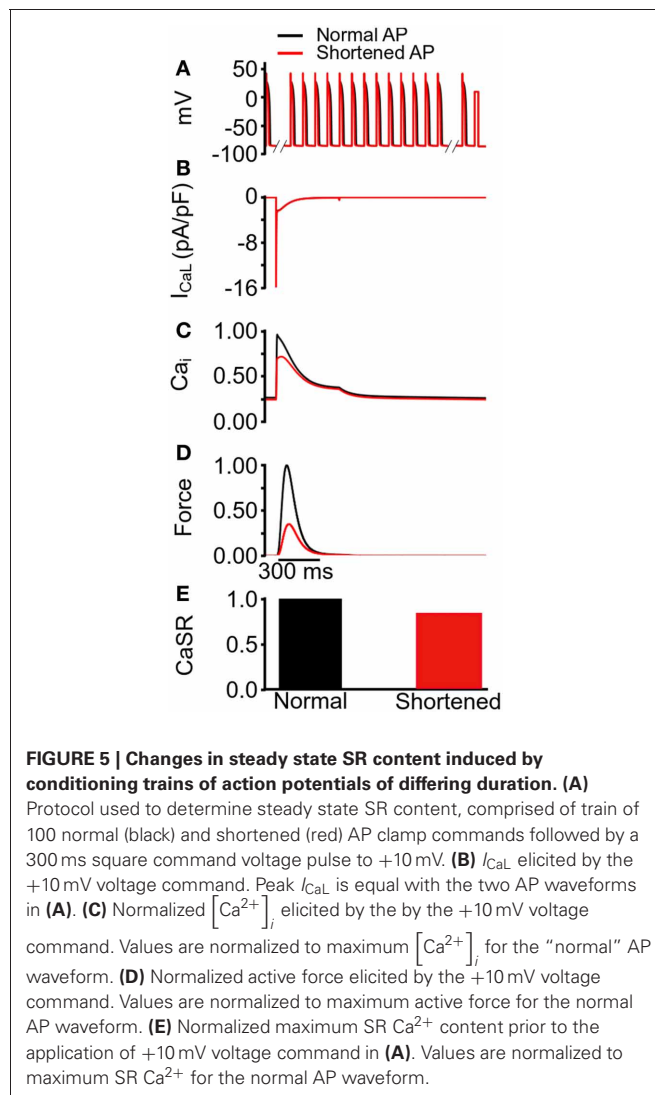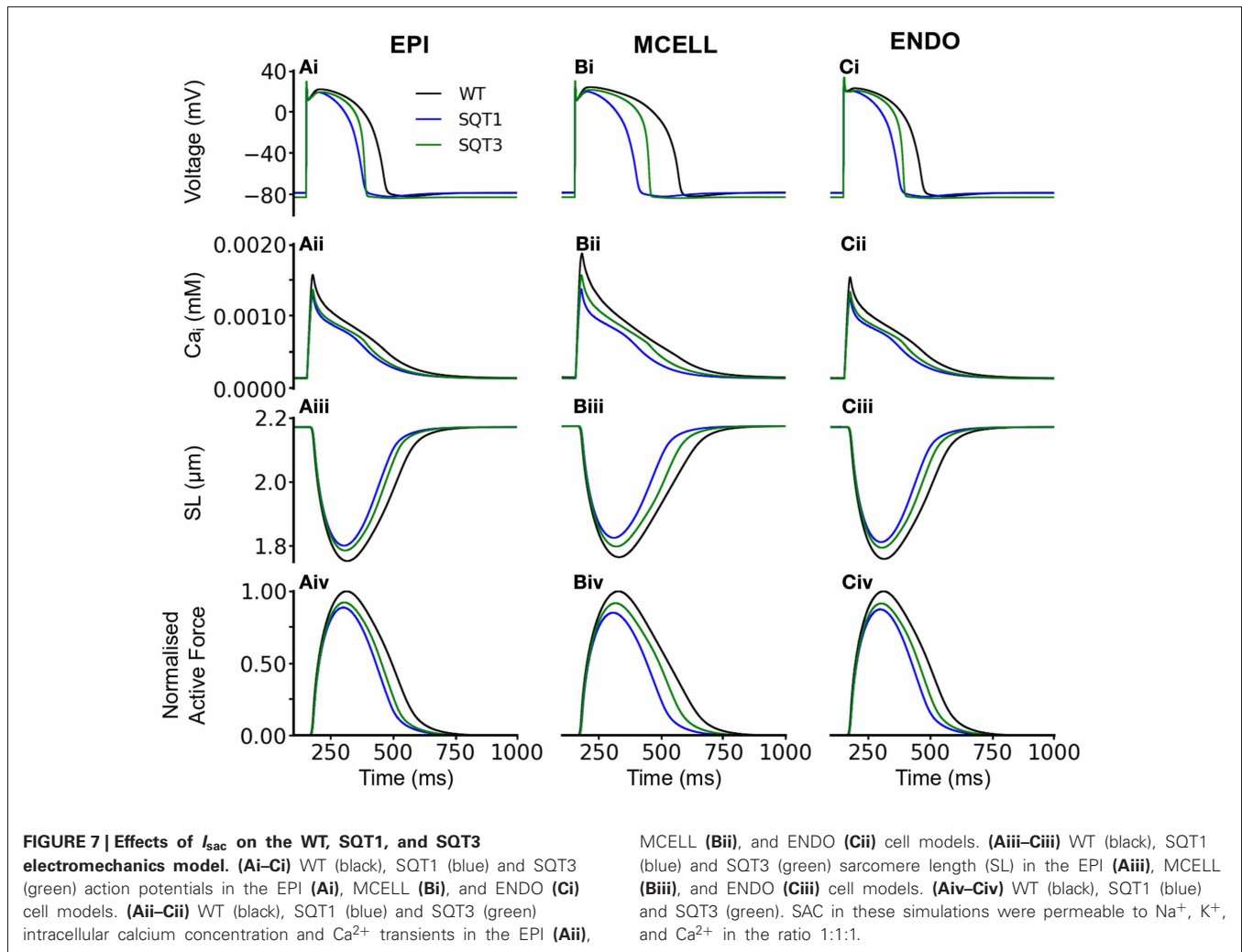
In order to investigate how I_{sac} attenuated the effects of the SQT1 and SQT3 mutations on $\left[Ca^{2+}\right]_i$ and cell contractility, a side-by-side comparison was made between the effects of the SQT1 and SQT3 mutations on AP duration, $\left[Ca^{2+}\right]_i$ and force production, in the absence of I_{sac} and with I_{sac} incorporated at the two permeability ratios (**Figure 8**). **Figures 8Ai–Ci** shows that the incorporation of I_{sac} at both permeability ratios reduced the APDs under the WT, SQT1 or SQT3 conditions, with a greater APD reduction in the case of permeability ratio of 1:1:1 than that of 1:1:0 as shown in **Table 1**. There was a greater $\left[Ca^{2+}\right]_i$ transient amplitude under both SQTS mutation conditions with the incorporation of I_{sac}; the greatest amplitude being at the 1:1:1 permeability ratio (**Figures 8Aii–Cii**). From **Figures 8Aiii–Ciii**, it is clear to see the increase in the $\left[Ca^{2+}\right]_i$ produced a greater SL shortening (relative to WT) on incorporation of I_{sac}, which consequently led to greater cell contractility in the SQT1 and SQT3 mutations particularly with a permeability ratio of 1:1:1 (**Figures 8Aiv–Civ**).

We then investigated how the incorporation of I_{sac} led to better maintenance of the $[Ca^{2+}]_i$ transient magnitude. **Figure 9** shows

FIGURE 6 | Effects of I_{sac} on the WT, SQT1, and SQT3 electromechanics model. (Ai–Ci) WT (black), SQT1 (blue) and SQT3 (green) action potentials in the EPI **(Ai)**, MCELL **(Bi)**, and ENDO **(Ci)** cell models. **(Aii–Cii)** WT (black), SQT1 (blue) and SQT3 (green) intracellular calcium concentration and Ca^{2+} transients in the EPI **(Aii)**, MCELL **(Bii)**, and ENDO **(Cii)** cell models. **(Aiii–Ciii)** WT (black), SQT1 (blue) and SQT3 (green) sarcomere length (SL) in the EPI **(Aiii)**, MCELL **(Biii)**, and ENDO **(Ciii)** cell models. **(Aiv–Civ)** WT (black), SQT1 (blue) and SQT3 (green). SAC in these simulations were permeable to Na^+, K^+, and Ca^{2+} in the ratio 1:1:0.

the computed APs (**Figures 9Ai–Ci**), I_{CaL} (**Figures 9Aii–Cii**), $[Na^+]_i$ (**Figures 9Aiii–Ciii**), $[Ca^{2+}]_i$ (**Figures 9Aiv–Civ**), CaSR (**Figures 9 Av–Cv**) and I_{NaCa} (**Figures 9 Avi–Cvi**) with and without I_{sac} (permeability ratio 1:1:1) in the WT, SQT1 and SQT2 conditions. Under the WT, SQT1 and SQT3 conditions, it was shown that incorporation of I_{sac} did not produce a noticeable change in the amplitude of I_{CaL}, but elevated $[Na^+]_i$, $[Ca^{2+}]_i$, and CaSR. These changes in the intracellular Na^+ and Ca^{2+} concentrations were associated with an altered I_{NaCa} as shown in **Figures 9Avi–Cvi**. In the case when I_{sac} was absent, during the initial depolarization phase of the AP, I_{NaCa} operated briefly in its reverse-mode that brought Ca^{2+} into the cytoplasmic space, producing an outward I_{NaCa}. During the plateau and early repolarization phases, I_{NaCa} remained almost zero for a period before switching to a forward mode to extrude Ca^{2+} out of cell cytoplasmic space, producing an inward I_{NaCa} current in the late repolarization phase. However, in the case with I_{sac}, the activation of I_{sac} brought more Na^+ into the cell cytoplasmic space (as it is permeable to Na^+) producing an elevated level of $[Na^+]_i$ (**Figures 9Aiii–Ciii**) as compared to the case when I_{sac} was absent. Consequently, I_{NaCa} operated longer in a reverse-mode

during the AP phase before it reverted to a normal mode in late repolarization phase. This led to a greater I_{NaCa} amplitude in both the reverse and forward modes (**Figures 9 Avi–Cvi**). A greater I_{NaCa} in the reverse-mode brought more Ca^{2+} into the cell cytoplasmic space, resulting in a higher systolic level of $[Ca^{2+}]_i$ (**Figures 9 Aiv–Civ**) and a greater level of the CaSR (**Figures 9Av–Cv**). Though this observation was *qualitatively* similar for the WT (**Figure 9Avi**), SQT1 (**Figure 9Bvi**) and SQT3 conditions (**Figure 9Cvi**), in *quantitative* terms the increase in the $[Ca^{2+}]_i$ was more dramatic in the SQT1 and 3 than WT settings. Thus, incorporation of I_{sac} into the simulations increased $[Ca^{2+}]_i$ by 88% under the WT condition, but by 153% under the SQT1 condition and by 94% under the SQT3 setting. The greater increase of $[Ca^{2+}]_i$ under the SQT simulation conditions provides an explanation for the maintenance of the Ca^{2+} transient by I_{sac}. Our simulated elevation of $[Na^+]_i$ by I_{sac} is consistent with previous experimental studies (Alvarez et al., 1999; Isenberg et al., 2003; Youm et al., 2005) that have shown an increase in cytosolic and total $[Na^+]_i$ by a mechanical stretch in human, mouse and ventricular myocytes, which has been attributed to the reverse-mode of I_{NaCa} during the rising phase of APs (Gannier et al., 1996;

FIGURE 7 | Effects of I_{sac} on the WT, SQT1, and SQT3 electromechanics model. (Ai–Ci) WT (black), SQT1 (blue) and SQT3 (green) action potentials in the EPI **(Ai)**, MCELL **(Bi)**, and ENDO **(Ci)** cell models. **(Aii–Cii)** WT (black), SQT1 (blue) and SQT3 (green) intracellular calcium concentration and Ca^{2+} transients in the EPI **(Aii)**, MCELL **(Bii)**, and ENDO **(Cii)** cell models. **(Aiii–Ciii)** WT (black), SQT1 (blue) and SQT3 (green) sarcomere length (SL) in the EPI **(Aiii)**, MCELL **(Biii)**, and ENDO **(Ciii)** cell models. **(Aiv–Civ)** WT (black), SQT1 (blue) and SQT3 (green). SAC in these simulations were permeable to Na^+, K^+, and Ca^{2+} in the ratio 1:1:1.

Alvarez et al., 1999; Calaghan and White, 1999; Kamkin et al., 2000, 2003; Calaghan et al., 2003; Youm et al., 2005).
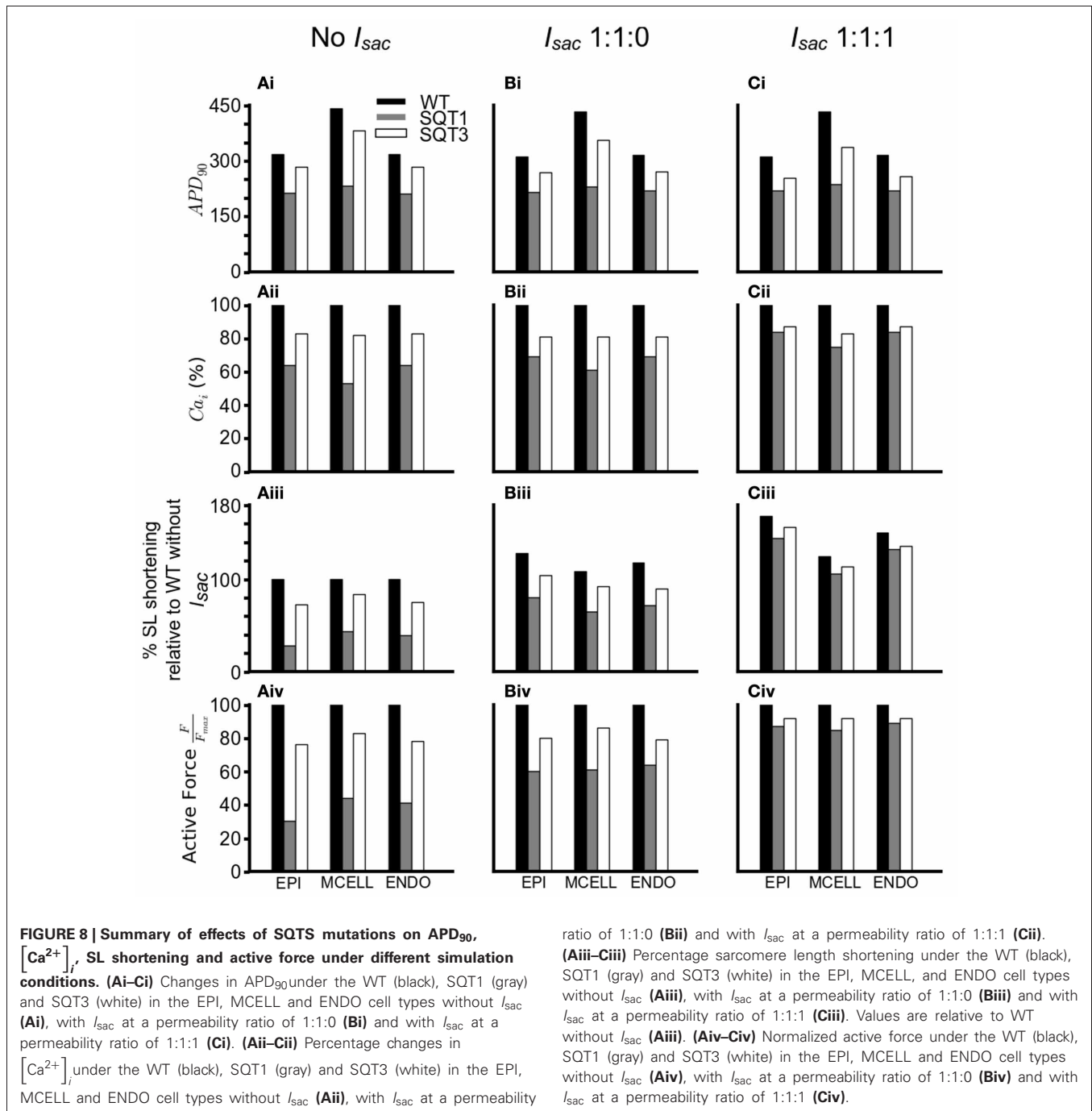
3D SIMULATIONS

Results from single cell models cannot be translated automatically to the intact tissue situation due to intercellular electrical coupling and mechanical deformation of tissue. Schimpf et al. (2008) observed a dissociation between ventricular repolarization and the end of mechanical systole in SQT patients. Consequently, to investigate this observation, we implemented a multi-cellular 3D tissue model of the human ventricles that considered the intercellular electrical coupling and mechanical deformation of tissue. Simulation results using the human ventricle 3D model are shown in **Figure 10**. **Figure 10A** shows the ventricles during diastole before contraction, whilst **Figure 10B** shows deformation under the WT condition; maximum deformation occurred at 230 ms. Maximum deformation occurred at 200 ms and 210 ms under the SQT1 (**Figure 10C**) and SQT3 (**Figure 10D**) conditions respectively but in contrast to WT, repolarization had already advanced significantly, particularly under the SQT1 condition. The vertical lines show that contraction was greatest in

the WT condition (**Figure 10B**) and least in the SQT1 setting (**Figure 10C**) but due to the incorporation of I_{sac}, contractility was not significantly impaired in either mutation condition, which agrees with available clinical evidence (Schimpf et al., 2008).

DISCUSSION

SUMMARY OF MAJOR FINDINGS

Electromechanical coupling in the heart is an active area of research and an important mechanism that couples electrical and mechanical processes is the presence of cardiac ion channels activated by mechanical stimuli such as changes in cell volume or cell stretch (Morris, 1990; Bustamante et al., 1991; Hagiwara et al., 1992; Van Wagoner, 1993; Suleymanian et al., 1995). In the present study, we have developed a family of multi-physical scale models for simulating the electromechanical coupling in the human ventricle at cellular and tissue levels under both WT and SQTS mutation conditions. Using these models we investigated the functional impact of AP abbreviation due to the SQT1 and SQT3 mutations on human ventricular mechanical dynamics. In the heart, SACs transduce mechanical energy into

FIGURE 8 | Summary of effects of SQTS mutations on APD$_{90}$, $[Ca^{2+}]_i$, SL shortening and active force under different simulation conditions. (Ai–Ci) Changes in APD$_{90}$ under the WT (black), SQT1 (gray) and SQT3 (white) in the EPI, MCELL and ENDO cell types without I_{sac} **(Ai)**, with I_{sac} at a permeability ratio of 1:1:0 **(Bi)** and with I_{sac} at a permeability ratio of 1:1:1 **(Ci)**. **(Aii–Cii)** Percentage changes in $[Ca^{2+}]_i$ under the WT (black), SQT1 (gray) and SQT3 (white) in the EPI, MCELL and ENDO cell types without I_{sac} **(Aii)**, with I_{sac} at a permeability ratio of 1:1:0 **(Bii)** and with I_{sac} at a permeability ratio of 1:1:1 **(Cii)**. **(Aiii–Ciii)** Percentage sarcomere length shortening under the WT (black), SQT1 (gray) and SQT3 (white) in the EPI, MCELL, and ENDO cell types without I_{sac} **(Aiii)**, with I_{sac} at a permeability ratio of 1:1:0 **(Biii)** and with I_{sac} at a permeability ratio of 1:1:1 **(Ciii)**. Values are relative to WT without I_{sac} **(Aiii)**. **(Aiv–Civ)** Normalized active force under the WT (black), SQT1 (gray) and SQT3 (white) in the EPI, MCELL and ENDO cell types without I_{sac} **(Aiv)**, with I_{sac} at a permeability ratio of 1:1:0 **(Biv)** and with I_{sac} at a permeability ratio of 1:1:1 **(Civ)**.

cellular responses and can carry considerable currents (Franz et al., 1992; Alvarez et al., 1999; Calaghan and White, 1999; Calaghan et al., 2003; Youm et al., 2005). Consequently, we incorporated a stretch-activated channel current (I_{sac}) into our single cell models to investigate the consequences of its inclusion under WT and SQTS mutation conditions. Our simulations suggest that: (i) at least *in silico*, abbreviated repolarization in the SQTS has the potential to reduce ventricular mechanical function; (ii) the inclusion of (I_{sac}) in the model acts to maintain the normal amplitude of the contractile force (**Figures 6–8**);

and (iii) there is a dissociation between ventricular repolarization and the end of mechanical systole in 3D SQTS simulations (**Figure 10**), which matches clinical observations by Schimpf et al. (2008). Several aspects of our findings merit more detailed discussion.

MECHANISTIC INSIGHTS
The results of simulated AP clamp experiments utilizing longer and shorter duration APs in the WT electromechanics model (**Figure 4**) provide mechanistic insight into the cause of the
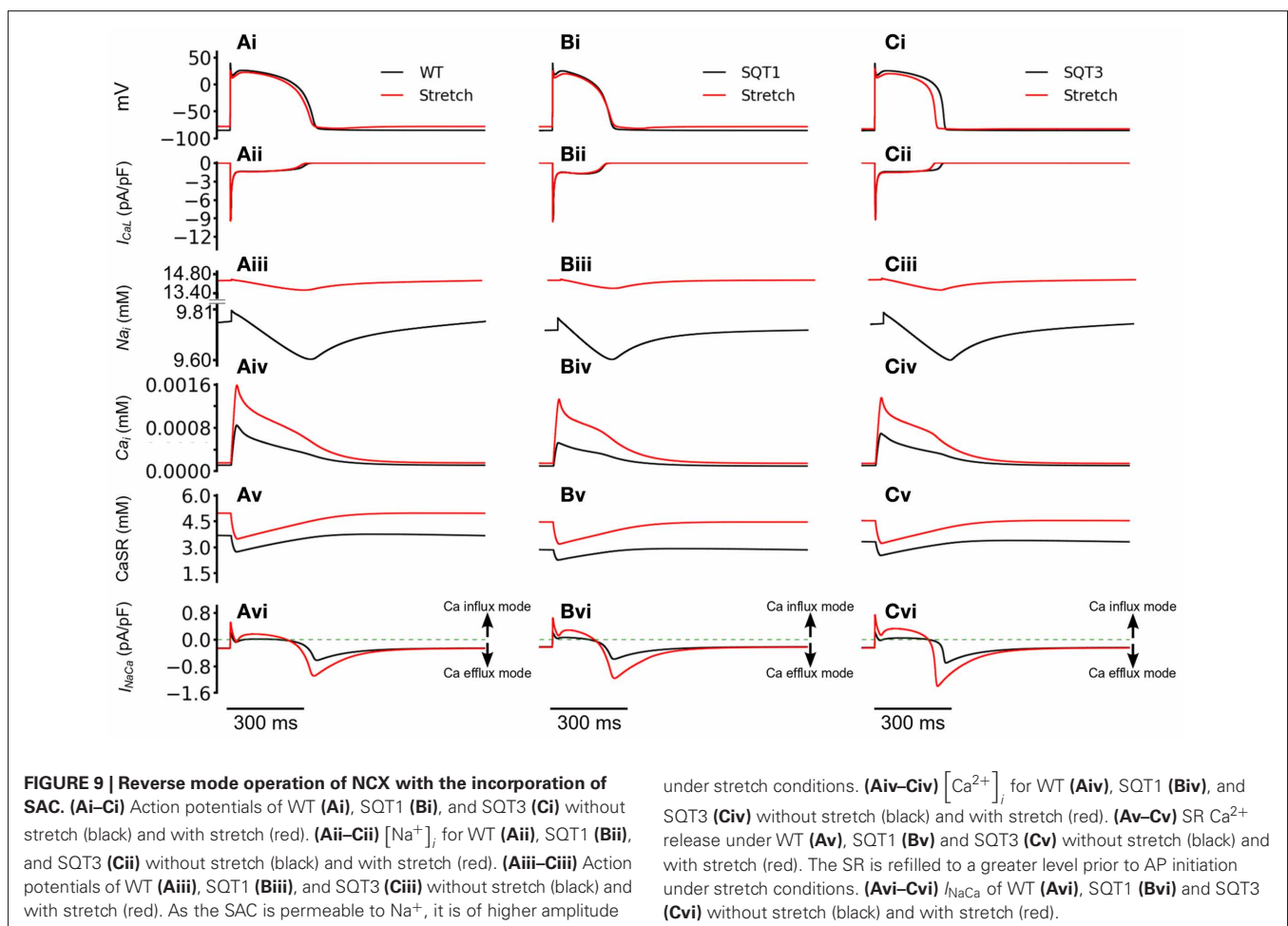
profound reduction and effects on contractility under simulated SQT1 and SQT3 conditions. In these simulations it was shown that markedly reduced contractility was attributable to reduced SR Ca^{2+} loading. AP shortening alters cellular electrical
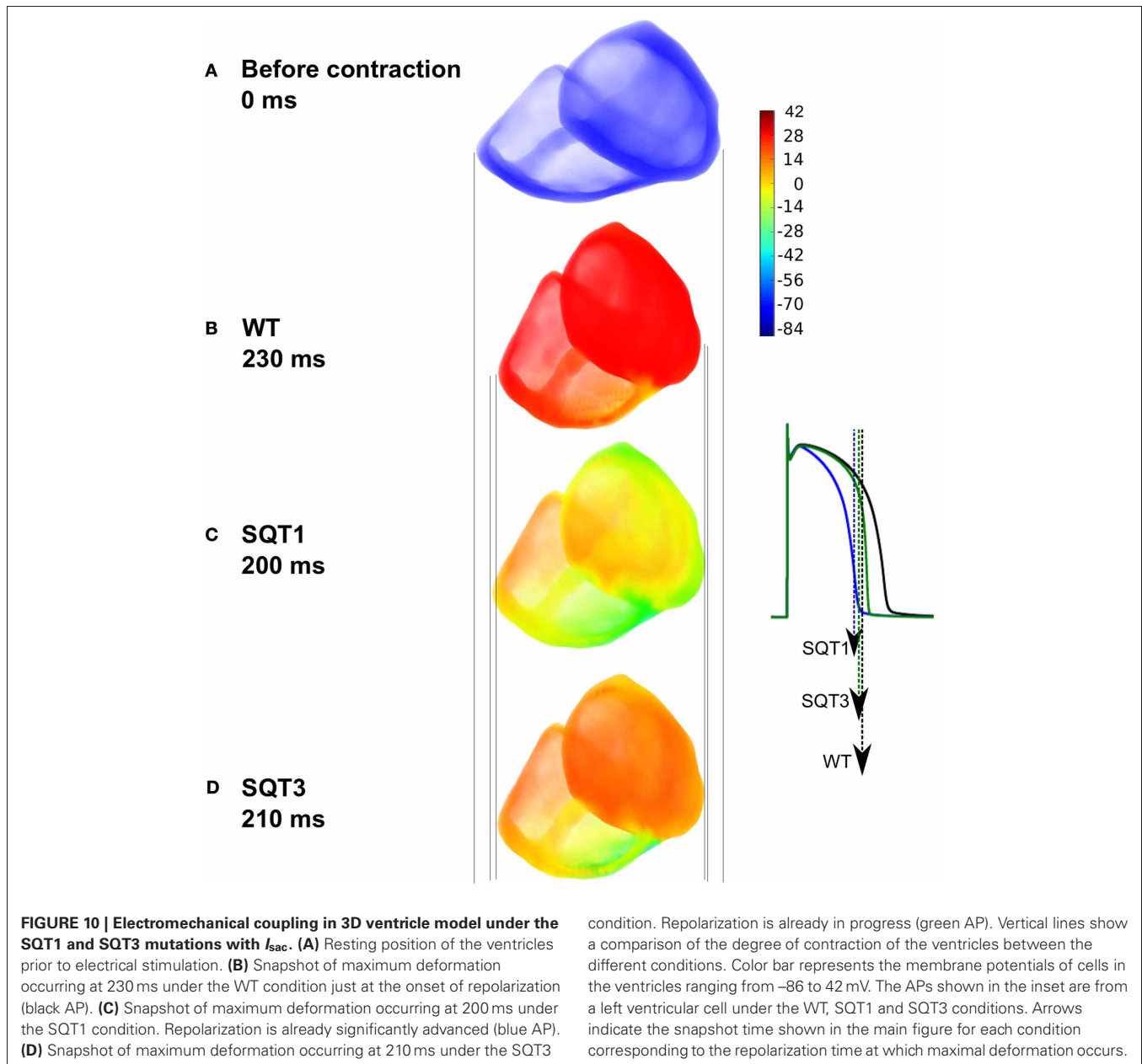
Table 1 | Changes in APD in the EPI, MCELL, and EDO cells with I_{sac}.

		APD (ms)		
		No I_{sac}	I_{sac} (Permeability 1:1:0)	I_{sac} (Permeability 1:1:1)
WT	EPI	317	310	306
	MCELL	441	433	420
	ENDO	317	314	310
SQT1	EPI	212	214	218
	MCELL	232	230	237
	ENDO	211	218	218
SQT3	EPI	283	269	253
	MCELL	382	355	336
	ENDO	284	270	257

dynamics and provides less time for SR Ca^{2+} loading and therefore SR Ca^{2+} content is compromised. This leads to a reduced SR Ca^{2+} release and, consequently, cell shortening. These observations are somewhat similar to previously reported effects of K-ATP channel openers. For example, K-ATP channel activation with lemakalim has been reported to reduce ventricular myocyte Ca^{2+} transients and contraction (Jiang et al., 1994), whilst a second K-ATP channel opener HOE 234 produced a negative inotropic effect on papillary muscle preparations (Kocić and Siluta, 1995).

Our simulation data are suggestive that the presence of SACs attenuates the reduced ventricular cell contractility arising from SQTS K channel mutations. This can be ascribed to the effects of I_{sac} on SR Ca^{2+} loading and therefore the amplitude of $\left[Ca^{2+}\right]_i$ transients as shown in **Figure 8**. With I_{sac}, with a Na:K:Ca ratio of either 1:1:0 or 1:1:1, there was a greater $\left[Ca^{2+}\right]_i$ transient amplitude and higher SR Ca^{2+} content, resulting in a greater shortening of the SL and active force as compared to the case when I_{sac} was absent. Such an effect of I_{sac} on the intracellular Ca^{2+} handling is due to two factors. First, during the depolarization phase of the AP, I_{NaCa} operates in a reverse mode that brings Ca^{2+} into the cytoplasmic space due to Na$^+$ influx. As I_{sac} is permeable to

FIGURE 9 | Reverse mode operation of NCX with the incorporation of SAC. (Ai–Ci) Action potentials of WT **(Ai)**, SQT1 **(Bi)**, and SQT3 **(Ci)** without stretch (black) and with stretch (red). **(Aii–Cii)** [Na$^+$]$_i$ for WT **(Aii)**, SQT1 **(Bii)**, and SQT3 **(Cii)** without stretch (black) and with stretch (red). **(Aiii–Ciii)** Action potentials of WT **(Aiii)**, SQT1 **(Biii)**, and SQT3 **(Ciii)** without stretch (black) and with stretch (red). As the SAC is permeable to Na$^+$, it is of higher amplitude under stretch conditions. **(Aiv–Civ)** $\left[Ca^{2+}\right]_i$ for WT **(Aiv)**, SQT1 **(Biv)**, and SQT3 **(Civ)** without stretch (black) and with stretch (red). **(Av–Cv)** SR Ca^{2+} release under WT **(Av)**, SQT1 **(Bv)** and SQT3 **(Cv)** without stretch (black) and with stretch (red). The SR is refilled to a greater level prior to AP initiation under stretch conditions. **(Avi–Cvi)** I_{NaCa} of WT **(Avi)**, SQT1 **(Bvi)** and SQT3 **(Cvi)** without stretch (black) and with stretch (red).

FIGURE 10 | Electromechanical coupling in 3D ventricle model under the SQT1 and SQT3 mutations with I_{sac}. (A) Resting position of the ventricles prior to electrical stimulation. **(B)** Snapshot of maximum deformation occurring at 230 ms under the WT condition just at the onset of repolarization (black AP). **(C)** Snapshot of maximum deformation occurring at 200 ms under the SQT1 condition. Repolarization is already significantly advanced (blue AP). **(D)** Snapshot of maximum deformation occurring at 210 ms under the SQT3 condition. Repolarization is already in progress (green AP). Vertical lines show a comparison of the degree of contraction of the ventricles between the different conditions. Color bar represents the membrane potentials of cells in the ventricles ranging from –86 to 42 mV. The APs shown in the inset are from a left ventricular cell under the WT, SQT1 and SQT3 conditions. Arrows indicate the snapshot time shown in the main figure for each condition corresponding to the repolarization time at which maximal deformation occurs.

Na$^+$, the activation of I_{sac} elevates $\left[\text{Na}^+\right]_i$, consequentially produces a greater reversed I_{NaCa} that elevates the $\left[\text{Ca}^{2+}\right]_i$ (**Figure 9**). The elevation of $\left[\text{Na}^+\right]_i$ leading to the reverse-mode of I_{NaCa} have been reported by previous studies (Bassingthwaighte et al., 1976; Eisner et al., 1983; Hume and Uehara, 1986; Barcenas-Ruiz et al., 1987; Gannier et al., 1996; Alvarez et al., 1999; Calaghan and White, 1999; Kamkin et al., 2000, 2003; Calaghan et al., 2003; Youm et al., 2005). Secondly, the increased $\left[\text{Ca}^{2+}\right]_i$ and the Ca^{2+} entry via I_{NaCa} in its reversed mode can both lead to more Ca^{2+} being pumped back to the SR, contributing to a greater CaSR, and trigger more SR Ca^{2+} release (Leblanc and Hume, 1990; Levesque et al., 1991; Litwin et al., 1996; Bers, 2001), thereby elevating [Ca^{2+}]$_i$ (**Figure 10**).

The dissociation between ventricular repolarization and the end of mechanical systole reflects the difference time course of the two processes. Our simulation data show that relative to ongoing mechanical contraction, ventricular repolarization terminates significantly earlier in SQTS conditions. Thus, accelerated repolarization in the SQTS exacerbates differences between electrical and mechanical events. By way of illustration, in our 3D anatomical human ventricle simulations, at the point of maximum deformation, repolarization was already underway in the SQT1 and SQT3 conditions (**Figure 10**) whereas it had not begun under the WT condition.

RELEVANCE TO PREVIOUS STUDIES

Our simulation data suggest that I_{sac} plays an important role in modulating cardiac electromechanical coupling. This is consistent with previous findings (Hirabayashi et al., 2008; Keldermann et al., 2010). In their study, Keldermann developed a coupled

electromechanical model for the left human ventricle, and used the model to investigate possible functional roles of I_{sac} on the re-entrant electrical wave conductions. It was found that mechanoelectrical feedback via I_{sac} can induce the deterioration of an otherwise stable spiral wave into turbulent wave patterns similar to that of ventricular fibrillation. A similar role for I_{sac} has also been observed in the study of (Hirabayashi et al., 2008). Findings from the present study add to these previous studies, in demonstrating the important role of I_{sac} in cardiac electromechanical dynamics.

In relation to the SQTS, Gaita et al. (2003) performed echocardiography, cardiac MRI and stress tests on the two families in which the SQTS was first reported (Gaita et al., 2003) and found no evident structural abnormalities. In subsequent work on mechanical function in the SQTS by Schimpf et al. (2008), no significant difference was seen between control subjects and SQTS patients in end systolic volume, end diastolic volume and ejection fraction. However, a dissociation between ventricular repolarization and the end of mechanical systole was observed. Our 3D simulations (**Figure 10**) qualitatively match and substantiate this clinical finding (Schimpf et al., 2008).

LIMITATIONS

In addition to acknowledged limitations of both the TP electrophysiology model (Ten Tusscher and Panfilov, 2006) and the Rice et al. (2008) mechanics model, although our coupled electromechanics model exhibited the Bowditch staircase or Treppe effect (Woodworth, 1902; Mulieri et al., 1992; Lakatta, 2004), it was only qualitatively able to reproduce experimental force-frequency characteristics. In simulations at increased pacing rates from 1.5 to 4 Hz, we observed APD shortening with an increase in the pacing rate, but due to reduced time for Ca^{2+} extrusion and SR accumulation between successive APs, there was an increase in the amplitude of the $\left[Ca^{2+}\right]_i$ transient and the active force in both WT and SQT settings. This was particularly the case at the faster rates examined, where there was insufficient time for restoration of Ca^{2+} dynamics between successive APs. These modeling observations require further validation and, if necessary, improvement in Ca^{2+} dynamics when experimental data become available. However, over the frequency range of 1–2 Hz our data matched reasonably experimental force-frequency data (**Figure 2**) and all simulations of the effects of SQT mutations presented here were conducted at 1 Hz. In the ventricular electrophysiology cell models, we did not consider the effects of β-adrenergic stimulation

or more physiologically-detailed Ca^{2+} handling mechanisms as implemented in some recently published models (Grandi et al., 2010; O'Hara et al., 2011). These effects may affect quantitatively the simulation results (Puglisi et al., 2013). Additionally, due to lack of experimental data on the I_{sac} in human ventricular myocytes, I_{sac} density was based on the study of (Panfilov et al., 2005; Youm et al., 2005; Kuijpers, 2008; Kohl and Sachs, 2001; Lunze et al., 2010). Whilst we have investigated the effects of I_{sac} on attenuation of force reduction in the SQTS setting, it is possible that alternative mechanisms may be involved such as calcium transport controlled by feedback of SR filling via store-operated Ca^{2+} channels (SOC) (Kusters et al., 2005; Kowalewski et al., 2006; Berna-Erro et al., 2012). Consequently, in additional simulations (data not shown), we have incorporated into the model a SOC channel current based on the Kuster et al. model (Kusters et al., 2005). In contrast to our findings with I_{sac}, with I_{SOC} incorporation no significant attenuation (<6%) of the force reduction in the SQTS settings was observed for the maximal SOC channel conductance varying from 0.2 to 20 pS/pF. Whilst it is important that these potential limitations are stated, they do not fundamentally alter the principal conclusions of this study.

CONCLUSION

Our tissue simulations qualitatively reproduce and provide a possible explanation for dissociation between the end of mechanical systole and ventricular repolarization (Schimpf et al., 2008): accelerated repolarization under SQTS conditions exacerbates differences in time-course between mechanical and electrical events. The results of the simulations in this study also raise a question as to whether electromechanical coupling involving I_{sac} offsets a negative inotropic effect of ventricular action potential abbreviation that might otherwise occur for K^+-channel linked SQTS. If, *in vivo*, I_{sac} does not execute such a role, then it is possible that other compensatory changes exist in SQTS patients as accelerated repolarization might otherwise result in altered SR Ca^{2+} loading and a reduction in contractile activity.

REFERENCES

Adeniran, I., El Harchi, A., Hancox, J. C., and Zhang, H. (2012). Proarrhythmia in KCNJ2-linked short QT syndrome - insights from modelling. *Cardiovasc. Res.* 94, 66–76. doi: 10.1093/cvr/cvs082

Adeniran, I., McPate, M. J. W., Witchel, H. J., Hancox, J. C., and Zhang, H. (2011). Increased vulnerability of human ventricle to re-entrant excitation in hERG-linked variant 1 short QT syndrome. *PLoS Comput. Biol.* 7:e1002313. doi: 10.1371/journal.pcbi.1002313

Alvarez, B. V., Pérez, N. G., Ennis, I. L., Camilión de Hurtado, M. C., and Cingolani, H. E. (1999). Mechanisms underlying the increase in force and Ca(2+) transient that follow stretch of cardiac muscle: a possible explanation of the Anrep effect. *Circ. Res.* 85, 716–722. doi: 10.1161/01.RES.85.8.716

Anttonen, O., Junttila, J., Giustetto, C., Gaita, F., Linna, E., Karsikas, M., et al. (2009). T-Wave morphology in short QT syndrome. *Ann. Noninvasive Electrocardiol.* 14,

262–267. doi: 10.1111/j.1542-474X.2009.00308.x

Antzelevitch, C., Pollevick, G. D., Cordeiro, J. M., Casis, O., Sanguinetti, M. C., Aizawa, Y., et al. (2007). Loss-of-function mutations in the cardiac calcium channel underlie a new clinical entity characterized by ST-segment elevation, short QT intervals, and sudden cardiac death. *Circulation* 115, 442–449. doi: 10.1161/CIRCULATIONAHA.106.668392

Barcenas-Ruiz, L., Beuckelmann, D. J., and Wier, W. G. (1987).

Sodium-calcium exchange in heart: membrane currents and changes in [Ca2+]$_i$. *Science* 238, 1720–1722. doi: 10.1126/science.3686010

Bassingthwaighte, J. B., Fry, C. H., and McGuigan, J. A. (1976). Relationship between internal calcium and outward current in mammalian ventricular muscle; a mechanism for the control of the action potential duration. *J. Physiol. (Lond.)* 262, 15–37.

Bellocq, C., van Ginneken, A. C. G., Bezzina, C. R., Alders, M., Escande, D., Mannens, M. M. A.

M., et al. (2004). Mutation in the KCNQ1 gene leading to the short QT-interval syndrome. *Circulation* 109, 2394–2397. doi: 10.1161/01. CIR.0000130409.72142.FE

Berna-Erro, A., Redondo, P. C., and Rosado, J. A. (2012). Store-operated Ca(2+) entry. *Adv. Exp. Med. Biol.* 740, 349–382. doi: 10.1007/978-94-007-2888-2_15

Bers, D. (2001). *Excitation-Contraction Coupling and Cardiac Contractile Force. 2nd Edn.* Dordrecht: Springer. doi: 10.1007/978-94-010-0658-3

Bett, G. C., and Sachs, F. (1997). Cardiac mechanosensitivity and stretch-activated ion channels. *Trends Cardiovasc. Med.* 7, 4–8. doi: 10.1016/S1050-1738(96)00119-3

Bogaert, J., and Rademakers, F. E. (2001). Regional nonuniformity of normal adult human left ventricle. *Am. J. Physiol. Heart Circ. Physiol.* 280, H610–H620.

Boland, J., and Troquet, J. (1980). Intracellular action potential changes induced in both ventricles of the rat by an acute right ventricular pressure overload. *Cardiovasc. Res.* 14, 735–740. doi: 10.1093/cvr/14.12.735

Bonet, J., and Wood, R. D. (2008). *Nonlinear Continuum Mechanics for Finite Element Analysis, 2nd Edn.* New York, NY: Cambridge University Press. doi: 10.1017/CBO9780511755446

Braess, D. (2007). *Finite Elements: Theory, Fast Solvers, and Applications in Solid Mechanics, 3rd Edn.* New York, NY: Cambridge University Press. doi: 10.1017/CBO9780511618635

Brenner, S. C., and Scott, R. (2010). *The Mathematical Theory of Finite Element Methods. Softcover Reprint of Hardcover, 3rd Edn. 2008.* New York, NY: Springer.

Brugada, R., Hong, K., Dumaine, R., Cordeiro, J., Gaita, F., Borggrefe, M., et al. (2004). Sudden death associated with short-QT syndrome linked to mutations in HERG. *Circulation* 109, 30–35. doi: 10.1161/01.CIR.0000109482.92774.3A

Burnett, D. S. (1987). *Finite Element Analysis: From Concepts to Applications, 1st Edn.* Reading, MA: Addison Wesley.

Bustamante, J. O., Ruknudin, A., and Sachs, F. (1991). Stretch-activated channels in heart cells: relevance to cardiac hypertrophy. *J. Cardiovasc. Pharmacol.* 17(Suppl. 2), S110–S113. doi: 10.1097/00005344-199117002-00024

Calaghan, S. C., Belus, A., and White, E. (2003). Do stretch-induced changes in intracellular calcium modify the electrical activity of cardiac muscle. *Prog. Biophys. Mol. Biol.* 82, 81–95. doi: 10.1016/S0079-6107(03)00007-5

Calaghan, S. C., and White, E. (1999). The role of calcium in the response of cardiac muscle to stretch. *Prog. Biophys. Mol. Biol.* 71, 59–90. doi: 10.1016/S0079-6107(98)00037-6

Chamberland, í., Fortin, A., and Fortin, M. (2010). Comparison of the performance of some finite element discretizations for large deformation elasticity problems. *Comput. Struct.* 88, 664–673.

Cheng, A., Nguyen, T. C., Malinowski, M., Daughters, G. T., Miller, D. C., and Ingels, N. B. Jr. (2008). Heterogeneity of left ventricular wall thickening mechanisms. *Circulation* 118, 713–721. doi: 10.1161/CIRCULATIONAHA. 107.744623

Cohen, S., Alan, and Hindmarsh, C. (1996). "Cvode, a stiff/nonstiff ode solver in, C.," in *C. Computers in Physics*, ed L. M. Holmes (New York, NY: American Institute of Physics Inc.), 138–143.

Colli Franzone, P., Pavarino, L. F., and Taccardi, B. (2005). Simulating patterns of excitation, repolarization and action potential duration with cardiac bidomain and monodomain models. *Math. Biosci.* 197, 35–66. doi: 10.1016/j.mbs.2005.04.003

Coppola, B. A., and Omens, J. H. (2008). Role of tissue structure on ventricular wall mechanics. *Mol. Cell. Biomech.* 5, 183–196.

Costa, K. D., Holmes, J. W., and Mcculloch, A. D. (2001). Modelling cardiac mechanical properties in three dimensions. *Phil. Trans. R. Soc. Lond. A* 359, 1233–1250. doi: 10.1098/rsta.2001.0828

Couderc, J.-P., and Lopes, C. M. (2010). Short and long QT syndromes: does QT length really matter. *J. Electrocardiol.* 43, 396–399. doi: 10.1016/j.jelectrocard.2010.07.009

Cross, B., Homoud, M., Link, M., Foote, C., Garlitski, A., Weinstock, J., et al. (2011). The short QT syndrome. *J. Int. Cardiac Electrophysiol.* 31, 25–31. doi: 10.1007/s10840-011-9566-0

Deo, M., Ruan, Y., Pandit, S. V., Shah, K., Berenfeld, O., Blaufox, A., et al. (2013). KCNJ2 mutation in short QT syndrome 3 results in atrial fibrillation and ventricular proarrhythmia. *Proc. Natl. Acad. Sci. U.S.A.* 110, 4291–4296. doi: 10.1073/pnas.1218154110

Eisner, D. A., Lederer, W. J., and Vaughan-Jones, R. D. (1983). The control of tonic tension by membrane potential and intracellular sodium activity in the sheep cardiac Purkinje fibre. *J. Physiol. (Lond.)* 335, 723–743.

Ern, A., and Guermond, J.-L. (2010). *Theory and Practice of Finite Elements. Softcover reprint of Hardcover, 1st Edn., 2004.* New York, NY: Springer.

Extramiana, F., and Antzelevitch, C. (2004). Amplified transmural dispersion of repolarization as the basis for arrhythmogenesis in a canine ventricular-wedge model of short-QT syndrome. *Circulation* 110, 3661–3666. doi: 10.1161/01. CIR.0000143078.48699.0C

Franz, M. R. (1996). Mechano-electrical feedback in ventricular myocardium. *Cardiovasc. Res.* 32, 15–24.

Franz, M. R., Cima, R., Wang, D., Profitt, D., and Kurz, R. (1992). Electrophysiological effects of myocardial stretch and mechanical determinants of stretch-activated arrhythmias. *Circulation* 86, 968–978. doi: 10.1161/01.CIR. 86.3.968

Gaita, F., Giustetto, C., Bianchi, F., Wolpert, C., Schimpf, R., Riccardi, R., et al. (2003). Short QT Syndrome: a familial cause of sudden death. *Circulation* 108, 965–970. doi: 10.1161/01.CIR. 0000085071.28695.C4

Gannier, F., White, E., Garnier, and Le Guennec, J. Y. (1996). A possible mechanism for large stretch-induced increase in $[Ca2+]_i$ in isolated guinea-pig ventricular myocytes. *Cardiovasc. Res.* 32, 158–167.

Gima, K., and Rudy, Y. (2002). Ionic current basis of electrocardiographic waveforms: a model study. *Circ. Res.* 90, 889–896. doi: 10.1161/01.RES.0000016960.61087.86

Giustetto, C., Di Monte, F., Wolpert, C., Borggrefe, M., Schimpf, R., Sbragia, P., et al. (2006). Short QT syndrome: clinical findings and diagnostic-therapeutic implications. *Eur. Heart J.* 27, 2440–2447. doi: 10.1093/eurheartj/ehl185

Gollob, M. H., Redpath, C. J., and Roberts, J. D. (2011). The short QT syndrome: proposed diagnostic criteria. *J. Am. Coll. Cardiol.* 57, 802–812. doi: 10.1016/j.jacc.2010.09.048

Grandi, E., Pasqualini, F. S., and Bers, D. M. (2010). A novel computational model of the human ventricular action potential and Ca transient. *J. Mol. Cell. Cardiol.* 48, 112–121. doi: 10.1016/j.yjmcc.2009.09.019

Guccione, J. M., McCulloch, A. D., and Waldman, L. K. (1991). Passive material properties of intact ventricular myocardium determined from a cylindrical model. *J. Biomech. Eng.* 113, 42–55. doi: 10.1115/1.2894084

Gussak, I., Brugada, P., Brugada, J., Wright, R. S., Kopecky, S. L., Chaitman, B. R., et al. (2000). Idiopathic short QT interval: a new clinical syndrome. *Cardiology* 94, 99–102. doi: 10.1159/000047299

Haga, J. B., Osnes, H., and Langtangen, H. P. (2012). On the causes of pressure oscillations in low-permeable and low-compressible porous media. *Int. J. Num. Anal. Methods Geomech.* 36, 1507–1522. doi: 10.1002/nag.1062

Hagiwara, N., Masuda, H., Shoda, M., and Irisawa, H. (1992). Stretch-activated anion currents of rabbit cardiac myocytes. *J. Physiol. (Lond.)* 456, 285–302.

Hancox, J. C., McPate, M. J., Harchi, A., Duncan, R. S., Dempsey, C. E., Witchel, H. J., et al. (2011). "The Short QT Syndrome," in *Heart Rate and Rhythm*, eds. O. N. Tripathi, U. Ravens, and M. C. Sanguinetti (Berlin, Heidelberg: Springer Berlin Heidelberg), 431–449. Available online at: http://www.springerlink. com/content/m8l86l8n3h81w43m/ [Accessed July 10, 2011].

Hattori, T., Makiyama, T., Akao, M., Ehara, E., Ohno, S., Iguchi, M., et al. (2011). A novel gain-of-function KCNJ2 mutation associated with short QT syndrome impairs inward rectification of Kir2.1 currents. *Cardiovas. Res.* 666–673. doi: 10.1093/cvr/cvr329

Hindmarsh, A. C., Brown, P. N., Grant, K. E., Lee, S. L., Serban, R., Shumaker, D. E., et al. (2005). SUNDIALS: suite of nonlinear and differential/algebraic equation solvers. *ACM Trans. Math. Softw.* 31, 363–396. doi: 10.1145/1089014. 1089020

Hirabayashi, S., Inagaki, M., and Hisada, T. (2008). Effects of wall stress on the dynamics of ventricular fibrillation: a simulation study using a dynamic mechanoelectric model of ventricular tissue. *J. Cardiovasc. Electrophysiol.* 19, 730–739. doi: 10.1111/j.1540-8167.2008.01099.x

Holzapfel, G. A. (2000). *Nonlinear Solid Mechanics: A Continuum Approach for Engineering, 1st Edn.* Chichester: Wiley.

Hong, K., Bjerregaard, P., Gussak, I., and Brugada, R. (2005a). Short QT syndrome and atrial fibrillation caused by mutation in KCNH2.

J. Cardiovasc. Electrophysiol 16, 394–396. doi: 10.1046/j.1540-8167.2005.40621.x

Hong, K., Piper, D. R., Diaz-Valdecantos, A., Brugada, J., Oliva, A., Burashnikov, E., et al. (2005b). De novo KCNQ1 mutation responsible for atrial fibrillation and short QT syndrome *in utero. Cardiovasc. Res.* 68, 433–440. doi: 10.1016/j.cardiores.2005.06.023

Hu, H., and Sachs, F. (1997). Stretch-activated ion channels in the heart. *J. Mol. Cell. Cardiol.* 29, 1511–1523. doi: 10.1006/jmcc.1997.0392

Hughes, T. J. R. (2000). *The Finite Element Method: Linear Static and Dynamic Finite Element Analysis.* New Jersey, NJ: Dover Publications.

Hume, J. R., and Uehara, A. (1986). "Creep currents" in single frog atrial cells may be generated by electrogenic Na/Ca exchange. *J. Gen. Physiol.* 87, 857–884. doi: 10.1085/jgp.87.6.857

Hunter, P. J., Nash, M. P., and Sands, G. B. (1997). "Computational Mechanics of the Heart," in *Computational Biology of the Heart,* eds A. V. Panfilov and A. V. Holden (West Sussex: Wiley), 345–407.

Isenberg, G., Kazanski, V., Kondratev, D., Gallitelli, M. F., Kiseleva, I., and Kamkin, A. (2003). Differential effects of stretch and compression on membrane currents and [Na+]c in ventricular myocytes. *Prog. Biophys. Mol. Biol.* 82, 43–56. doi: 10.1016/S0079-6107(03)00004-X

Jiang, C., Mochizuki, S., Poole-Wilson, P. A., Harding, S. E., and MacLeod, K. T. (1994). Effect of lemakalim on action potentials, intracellular calcium, and contraction in guinea pig and human cardiac myocytes. *Cardiovasc. Res.* 28, 851–857. doi: 10.1093/cvr/28.6.851

Kamkin, A., Kiseleva, I., and Isenberg, G. (2000). Stretch-activated currents in ventricular myocytes: amplitude and arrhythmogenic effects increase with hypertrophy. *Cardiovasc. Res.* 48, 409–420. doi: 10.1016/S0008-6363(00)00208-X

Kamkin, A., Kiseleva, I., and Isenberg, G. (2003). Ion selectivity of stretch-activated cation currents in mouse ventricular myocytes. *Pflugers Arch.* 446, 220–231.

Keener, J., and Sneyd, J. (2008). *Mathematical Physiology: II: Systems Physiology, 2nd Edn.* New York, NY: Springer.

Keldermann, R. H., Nash, M. P., Gelderblom, H., Wang, V. Y., and Panfilov, A. V. (2010). Electromechanical wavebreak

in a model of the human left ventricle. *Am. J. Physiol. Heart Circ. Physiol.* 299, H134–H143. doi: 10.1152/ajpheart.00862.2009

Keller, D. U. J., Kalayciyan, R., Dössel, O., and Seemann, G. (2009). "Fast creation of endocardial stimulation profiles for the realistic simulation of body surface ECGs," in *IFMBE Proceedings,* 145–148. Available online at: http://www.scopus.com/inward/record.url?eid=2-s2.0-77950134835andpartnerID=40andmd5=2db2b89cc19de5e28ec01ebbf0dffff0 [Accessed July 20, 2011]. doi: 10.1007/978-3-642-03882-2_37

Kocić, I., and Siluta, W. (1995). Cardiopharmacological profile of HOE 234, the new activator of ATP-sensitive K+ channels in the guinea pig heart. *Pol. J. Pharmacol.* 47, 457–460.

Kohl, P., Hunter, P., and Noble, D. (1999). Stretch-induced changes in heart rate and rhythm: clinical observations, experiments and mathematical models. *Prog. Biophys. Mol. Biol.* 71, 91–138. doi: 10.1016/S0079-6107(98)00038-8

Kohl, P., and Sachs, F. (2001). Mechanoelectric feedback in cardiac cells. *Phil. Trans. R. Soc. Lond. A* 359, 1173–1185. doi: 10.1098/rsta.2001.0824

Kowalewski, J. M., Uhlén, P., Kitano, H., and Brismar, H. (2006). Modeling the impact of store-operated Ca2+ entry on intracellular Ca2+ oscillations. *Math. Biosci.* 204, 232–249. doi: 10.1016/j.mbs.2006.03.001

Kuijpers, N. H. L. (2008). *Cardiac Electrophysiology and Mechanoelectric Feedback.* PhD thesis. Eindhoven: Eindhoven University of Technology.

Kusters, J. M. A. M., Dernison, M. M., van Meerwijk, W. P. M., Ypey, D. L., Theuvenet, A. P. R., and Gielen, C. C. A. M. (2005). Stabilizing role of calcium store-dependent plasma membrane calcium channels in action-potential firing and intracellular calcium oscillations. *Biophys. J.* 89, 3741–3756. doi: 10.1529/biophysj.105.062984

Lab, M. J. (1982). Contraction-excitation feedback in myocardium. *Physiol. Basis Clin. Relevance. Circ. Res.* 50, 757–766. doi: 10.1161/01.RES.50.6.757

Lab, M. J. (1996). Mechanoelectric feedback (transduction) in heart: concepts and implications. *Cardiovasc. Res.* 32, 3–14.

Lakatta, E. G. (2004). Beyond Bowditch: the convergence of

cardiac chronotropy and inotropy. *Cell Calcium* 35, 629–642. doi: 10.1016/j.ceca.2004.01.017

Land, S., Niederer, S. A., and Smith, N. P. (2012). Efficient computational methods for strongly coupled cardiac electromechanics. *IEEE Trans. Biomed. Eng.* 59, 1219–1228. doi: 10.1109/TBME.2011.2112359

Leblanc, N., and Hume, J. R. (1990). Sodium current-induced release of calcium from cardiac sarcoplasmic reticulum. *Science* 248, 372–376. doi: 10.1126/science.2158146

Legrice, I. J., Hunter, P. J., and Smaill, B. H. (1997). Laminar structure of the heart: a mathematical model. *Am. J. Physiol.* 272, H2466–H2476.

Levesque, P. C., Leblanc, N., and Hume, J. R. (1991). Role of reverse-mode Na(+)-Ca2+ exchange in excitation-contraction coupling in the heart. *Ann. N.Y. Acad. Sci.* 639, 386–397. doi: 10.1111/j.1749-6632.1991.tb17327.x

Lilli, A., Baratto, M. T., Meglio, J. D., Chioccioli, M., Magnacca, M., Talini, E., et al. (2013). Left ventricular rotation and twist assessed by four-dimensional speckle tracking echocardiography in healthy subjects and pathological remodeling: a single center experience. *Echocardiography* 30, 171–179. doi: 10.1111/echo.12026

Lions, J. L., and Ciarlet, P. G. (1994). *Handbook of Numerical Analysis; Vol.3, Techniques of Scientific Computing (part 1); Numerical methods for solids (part 1); Solution of equations in R(n) (part 2).* London: North-Holland Available online at: http://catalogue.library.manchester.ac.uk/items/815424 [Accessed April 25, 2013].

Litwin, S., Kohmoto, O., Levi, A. J., Spitzer, K. W., and Bridge, J. H. (1996). Evidence that reverse Na-Ca exchange can trigger SR calcium release. *Ann. N.Y. Acad. Sci.* 779, 451–463. doi: 10.1111/j.1749-6632.1996.tb44820.x

Logg, A., Mardal, K.-A., and Wells, G. eds. (2012). *Automated Solution of Differential Equations by the Finite Element Method: The FEniCS Book. 2012th Edn.* Heidelberg: Springer.

Lorenz, C. H., Pastorek, J. S., and Bundy, J. M. (2000). Delineation of normal human left ventricular twist throughout systole by tagged cine magnetic resonance imaging. *J. Cardiovasc. Magn. Reson.* 2, 97–108. doi: 10.3109/10976640009148678

Lunze, K., Stålhand, J., and Leonhardt, S. (2010). "Modeling of stretch-activated sarcolemmal channels in smooth muscle cells," in *World Congress on Medical Physics and Biomedical Engineering, September 7 - 12 2009, Munich, Germany IFMBE Proceedings,* eds O. Dössel and W. C. Schlegel (Springer Berlin Heidelberg), 740–743. Available online at: http://www.springerlink.com/content/k3052r8670832k70/abstract/ [Accessed September 20, 2012].

MacGowan, G. A., Shapiro, E. P., Azhari, H., Siu, C. O., Hees, P. S., Hutchins, G. M., et al. (1997). Noninvasive measurement of shortening in the fiber and cross-fiber directions in the normal human left ventricle and in idiopathic dilated cardiomyopathy. *Circulation* 96, 535–541. doi: 10.1161/01.CIR.96.2.535

Marsden, J. E., and Hughes, T. J. R. (1994). *Mathematical Foundations of Elasticity.* New Jersey, NJ: Dover Publications.

McIntosh, M. A., Cobbe, S. M., and Smith, G. L. (2000). Heterogeneous changes in action potential and intracellular Ca2+ in left ventricular myocyte sub-types from rabbits with heart failure. *Cardiovasc. Res.* 45, 397–409. doi: 10.1016/S0008-6363(99)00360-0

Morris, C. E. (1990). Mechanosensitive ion channels. *J. Membr. Biol.* 113, 93–107. doi: 10.1007/BF01872883

Mulieri, L. A., Hasenfuss, G., Leavitt, B., Allen, P. D., and Alpert, N. R. (1992). Altered myocardial force-frequency relation in human heart failure. *Circulation* 85, 1743–1750. doi: 10.1161/01.CIR.85.5.1743

Nash, M. P., and Panfilov, A. V. (2004). Electromechanical model of excitable tissue to study reentrant cardiac arrhythmias. *Prog. Biophys. Mol. Biol.* 85, 501–522. doi: 10.1016/j.pbiomolbio.2004.01.016

Niederer, S. A., and Smith, N. P. (2008). An improved numerical method for strong coupling of excitation and contraction models in the heart. *Prog. Biophys. Mol. Biol.* 96, 90–111. doi: 10.1016/j.pbiomolbio.2007.08.001

O'Hara, T., Virág, L., Varró, A., and Rudy, Y. (2011). Simulation of the undiseased human cardiac ventricular action potential: model formulation and experimental validation. *PLoS Comput. Biol.* 7: e1002061. doi: 10.1371/journal.pcbi.1002061

Panfilov, A. V., Keldermann, R. H., and Nash, M. P. (2005). Self-organized pacemakers in a coupled reaction-diffusion-mechanics system. *Phys.*

Rev. Lett. 95, 258104. doi: 10.1103/PhysRevLett.95.258104

Patel, C., and Antzelevitch, C. (2008). Cellular basis for arrhythmogenesis in an experimental model of the SQT1 form of the short QT syndrome. *Heart Rhythm* 5, 585–590. doi: 10.1016/j.hrthm.2008.01.022

Patel, U., and Pavri, B. B. (2009). Short QT syndrome: a review. *Cardiol. Rev.* 17, 300–303. doi: 10.1097/CRD. 0b013e3181c07592

Pathmanathan, P., and Whiteley, J. P. (2009). A numerical method for cardiac mechanoelectric simulations. *Ann. Biomed. Eng.* 37, 860–873. doi: 10.1007/s10439-009-9663-8

Potse, M., Dubé, B., Richer, J., Vinet, A., and Gulrajani, R. M. (2006). A comparison of monodomain and bidomain reaction-diffusion models for action potential propagation in the human heart. *IEEE Trans. Biomed. Eng.* 53, 2425–2435. doi: 10.1109/TBME.2006.880875

Priori, S. G., Pandit, S. V., Rivolta, I., Berenfeld, O., Ronchetti, E., Dhamoon, A., et al. (2005). A novel form of short QT syndrome (SQT3) is caused by a mutation in the KCNJ2 gene. *Circ. Res* 96, 800–807. doi: 10.1161/01.RES.0000162101.76263.8c

Puglisi, J. L., Negroni, J. A., Chen-Izu, Y., and Bers, D. M. (2013). The force-frequency relationship: insights from mathematical modeling. *Adv. Physiol. Educ.* 37, 28–34. doi: 10.1152/advan.00072.2011

Rice, J. J., Wang, F., Bers, D. M., and de Tombe, P. P. (2008). Approximate model of cooperative activation and crossbridge cycling in cardiac muscle using ordinary differential equations. *Biophys. J.* 95, 2368–2390. doi: 10.1529/biophysj.107.119487

Rush, S., and Larsen, H. (1978). A practical algorithm for solving dynamic membrane equations. *IEEE Trans. Biomed. Eng.* 25, 389–392. doi: 10.1109/TBME.1978.326270

Schimpf, R., Antzelevitch, C., Haghi, D., Giustetto, C., Pizzuti, A., Gaita, F., et al. (2008). Electromechanical coupling in patients with the short QT syndrome: further insights into the mechanoelectrical hypothesis of the U wave. *Heart Rhythm* 5, 241–245. doi: 10.1016/j.hrthm.2007.10.015

Schimpf, R., Wolpert, C., Gaita, F., Giustetto, C., and Borggrefe, M. (2005). Short QT syndrome. *Cardiovasc. Res* 67, 357–366. doi: 10.1016/j.cardiores.2005.03.026

Seemann, G., Keller, D. U. J., Weiss, D. L., and Dössel, O. (2006). "Modeling human ventricular geometry and fiber orientation based on diffusion tensor MRI," in *Computers in Cardiology*, 801–804. Available online at: http://www.scopus.com/inward/record.url?eid=2-s2.0-38049006338andpartnerID=40andmd5=d7c99be0309654b17513e9b39ee96029 [Accessed July 20, 2011].

Suleymanian, M. A., Clemo, H. F., Cohen, N. M., and Baumgarten, C. M. (1995). Stretch-activated channel blockers modulate cell volume in cardiac ventricular myocytes. *J. Mol. Cell. Cardiol.* 27, 721–728. doi: 10.1016/S0022-2828(08)80062-4

Sun, Y., Quan, X.-Q., Fromme, S., Cox, R. H., Zhang, P., Zhang, L., et al. (2011). A novel mutation in the KCNH2 gene associated with short QT syndrome. *J. Mol. Cell. Cardiol.* 50, 433–441. doi: 10.1016/j.yjmcc.2010.11.017

Sundnes, J., Lines, G. T., and Tveito, A. (2005). An operator splitting method for solving the bidomain equations coupled to a volume conductor model for the torso. *Math. Biosci.* 194, 233–248. doi: 10.1016/j.mbs.2005.01.001

Taggart, P. (1996). Mechano-electric feedback in the human heart. *Cardiovasc. Res.* 32, 38–43.

Taggart, P., Sutton, P. M., Opthof, T., Coronel, R., Trimlett, R., Pugsley, W., et al. (2000). Inhomogeneous transmural conduction during early ischaemia in patients with coronary artery disease. *J. Mol. Cell. Cardiol* 32, 621–630. doi: 10.1006/jmcc.2000.1105

Templin, C., Ghadri, J.-R., Rougier, J.-S., Baumer, A., Kaplan, V., Albesa, M., et al. (2011). Identification of a novel loss-of-function calcium channel gene mutation in short QT syndrome (SQTS6). *Eur. Heart J.* 32, 1077–1088. doi: 10.1093/eurheartj/ehr076

Trayanova, N., Li, W., Eason, J., and Kohl, P. (2004). Effect of stretch-activated channels on defibrillation efficacy. *Heart Rhythm* 1, 67–77. doi: 10.1016/j.hrthm.2004.01.002

Tseng, W.-Y. I., Reese, T. G., Weisskoff, R. M., Brady, T. J., and Wedeen, V. J. (2000). Myocardial fiber shortening in humans: Initial results of MR imaging. *Radiology* 216, 128–139.

Ten Tusscher, K. H. W. J., Noble, D., Noble, P. J., and Panfilov, A. V. (2004). A model for human ventricular tissue. *Am. J. Physiol. Heart Circ. Physiol* 286, H1573–H1589. doi: 10.1152/ajpheart.00794.2003

Ten Tusscher, K. H. W. J., and Panfilov, A. V. (2006). Alternans and spiral breakup in a human ventricular tissue model. *Am. J. Physiol. Heart Circ. Physiol* 291, H1088–H1100. doi: 10.1152/ajpheart.00109.2006

Van Wagoner, D. R. (1993). Mechanosensitive gating of atrial ATP-sensitive potassium channels. *Circ. Res.* 72, 973–983. doi: 10.1161/01.RES.72.5.973

Weiss, D. L., Seemann, G., Sachse, F. B., and Dössel, O. (2005). Modelling of short QT syndrome in a heterogeneous model of the human ventricular wall. *Europace* 7(Suppl. 2), 105–117. doi: 10.1016/j.eupc.2005.04.008

Whiteley, J. P., Bishop, M. J., and Gavaghan, D. J. (2007). Soft tissue modelling of cardiac fibres for use in coupled mechano-electric simulations. *Bull. Math. Biol.* 69, 2199–2225. doi: 10.1007/s11538-007-9213-1

Woodworth, R. S. (1902). Maximal contraction, "staircase" contraction, refractory period, and compensatory pause, of the heart. *Am. J. Physiol.* 8, 213–249.

Xia, L., Zhang, Y., Zhang, H., Wei, Q., Liu, F., and Crozier, S. (2006). Simulation of Brugada syndrome using cellular and three-dimensional whole-heart modeling approaches. *Physiol. Meas.* 27, 1125–1142. doi: 10.1088/0967-3334/27/11/006

Youm, J. B., Han, J., Kim, N., Zhang, Y.-H., Kim, E., Leem, C. H., et al. (2005). "role of stretch-activated channels in the heart: action potential and Ca2+ transients - mechanosensitivity in cells and tissues - NCBI bookshelf," in eds A. Kamkin and I. Kiseleva (Moscow: Academia). Available online at: http://www.ncbi.nlm.nih.gov/books/NBK7490/ [Accessed September 15, 2012].

Zabel, M., Koller, B. S., Sachs, F., and Franz, M. R. (1996). Stretch-induced voltage changes in the isolated beating heart: importance of the timing of stretch and implications for stretch-activated ion channels. *Cardiovasc. Res.* 32, 120–130.

Zhang, H., and Hancox, J. C. (2004). *In silico* study of action potential and QT interval shortening due to loss of inactivation of the cardiac rapid delayed rectifier potassium current. *Biochem. Biophys. Res. Commun.* 322, 693–699. doi: 10.1016/j.bbrc.2004.07.176

Zhang, H., Kharche, S., Holden, A. V., and Hancox, J. C. (2008). Repolarisation and vulnerability to re-entry in the human heart with short QT syndrome arising from KCNQ1 mutation–a simulation study. *Prog. Biophys. Mol. Biol* 96, 112–131. doi: 10.1016/j.pbiomolbio.2007.07.020

Conflict of Interest Statement: The authors declare that the research was conducted in the absence of any commercial or financial relationships that could be construed as a potential conflict of interest.